



Erlotinib alone or with bevacizumab as first-line therapy in patients with advanced non-squamous non-small-cell lung cancer harbouring *EGFR* mutations (J025567): an open-label, randomised, multicentre, phase 2 study

Takashi Seto, Terufumi Kato, Makoto Nishio, Koichi Goto, Shinji Atagi, Yukio Hosomi, Noboru Yamamoto, Toyooki Hida, Makoto Maemondo, Kazuhiko Nakagawa, Seisuke Nagase, Isamu Okamoto, Takeharu Yamanaka, Kosei Tajima, Ryosuke Harada, Masahiro Fukuoka, Nobuyuki Yamamoto

Summary

Background With use of *EGFR* tyrosine-kinase inhibitor monotherapy for patients with activating *EGFR* mutation-positive non-small-cell lung cancer (NSCLC), median progression-free survival has been extended to about 12 months. Nevertheless, new strategies are needed to further extend progression-free survival and overall survival with acceptable toxicity and tolerability for this population. We aimed to compare the efficacy and safety of the combination of erlotinib and bevacizumab compared with erlotinib alone in patients with non-squamous NSCLC with activating *EGFR* mutation-positive disease.

Methods In this open-label, randomised, multicentre, phase 2 study, patients from 30 centres across Japan with stage IIIB/IV or recurrent non-squamous NSCLC with activating *EGFR* mutations, Eastern Cooperative Oncology Group performance status 0 or 1, and no previous chemotherapy for advanced disease received erlotinib 150 mg/day plus bevacizumab 15 mg/kg every 3 weeks or erlotinib 150 mg/day monotherapy as a first-line therapy until disease progression or unacceptable toxicity. The primary endpoint was progression-free survival, as determined by an independent review committee. Randomisation was done with a dynamic allocation method, and the analysis used a modified intention-to-treat approach, including all patients who received at least one dose of study treatment and had tumour assessment at least once after randomisation. This study is registered with the Japan Pharmaceutical Information Center, number JapicCTI-111390.

Findings Between Feb 21, 2011, and March 5, 2012, 154 patients were enrolled. 77 were randomly assigned to receive erlotinib and bevacizumab and 77 to erlotinib alone, of whom 75 patients in the erlotinib plus bevacizumab group and 77 in the erlotinib alone group were included in the efficacy analyses. Median progression-free survival was 16·0 months (95% CI 13·9–18·1) with erlotinib plus bevacizumab and 9·7 months (5·7–11·1) with erlotinib alone (hazard ratio 0·54, 95% CI 0·36–0·79; log-rank test $p=0\cdot0015$). The most common grade 3 or worse adverse events were rash (19 [25%] patients in the erlotinib plus bevacizumab group vs 15 [19%] patients in the erlotinib alone group), hypertension (45 [60%] vs eight [10%]), and proteinuria (six [8%] vs none). Serious adverse events occurred at a similar frequency in both groups (18 [24%] patients in the erlotinib plus bevacizumab group and 19 [25%] patients in the erlotinib alone group).

Interpretation Erlotinib plus bevacizumab combination could be a new first-line regimen in *EGFR* mutation-positive NSCLC. Further investigation of the regimen is warranted.

Funding Chugai Pharmaceutical Co Ltd.

Introduction

Lung cancer is a leading cause of death worldwide; it is the primary cause of cancer deaths in men and the secondary cause in women.¹ Most patients with lung cancer have non-small-cell lung cancer (NSCLC) and a clinically significant proportion of patients have activating mutations of *EGFR*.² In this subgroup of patients, *EGFR* tyrosine-kinase inhibitors have consistently led to better outcomes than has standard chemotherapy.^{3–6} Erlotinib and gefitinib have been shown to prolong progression-free survival compared with chemotherapy in several phase 3 trials.^{7–10} Unfortunately, most patients with NSCLC with activating *EGFR* mutations who are given *EGFR* tyrosine-kinase

inhibitors eventually develop resistance and relapse within about 1 year of initiation of treatment.^{5,7–11} To improve outcomes, the foundation treatment of *EGFR* tyrosine-kinase inhibitors should be built on through investigation of biologically synergistic combinations.

The anti-angiogenic monoclonal antibody bevacizumab targets the VEGF signalling pathway and has been shown to provide additional efficacy when used in combination with first-line platinum-based chemotherapy in several trials in non-squamous NSCLC.^{12–14} The combination of erlotinib and bevacizumab has the potential to prolong progression-free survival in unselected populations of patients with NSCLC.^{15,16} In a subgroup analysis of *EGFR*

Lancet Oncol 2014

Published Online

August 28, 2014

[http://dx.doi.org/10.1016/S1470-2045\(14\)70381-X](http://dx.doi.org/10.1016/S1470-2045(14)70381-X)

See Online/Comment

[http://dx.doi.org/10.1016/S1470-2045\(14\)70386-9](http://dx.doi.org/10.1016/S1470-2045(14)70386-9)

National Kyushu Cancer Center, Fukuoka, Japan (T Seto MD); Kanagawa Cardiovascular and Respiratory Center, Kanagawa, Japan (T Kato MD); The Cancer Institute Hospital of the Japanese Foundation for Cancer Research, Tokyo, Japan (M Nishio MD); National Cancer Center Hospital East, Chiba, Japan (K Goto MD); Kinki-chuo Chest Medical Center, Osaka, Japan (S Atagi MD); Tokyo Metropolitan Cancer and Infectious Diseases Center Komagome Hospital, Tokyo, Japan (Y Hosomi MD); National Cancer Center Hospital, Tokyo, Japan (Noboru Yamamoto MD); Aichi Cancer Center, Aichi, Japan (T Hida MD); Miyagi Cancer Center, Miyagi, Japan (M Maemondo MD); Kinki University Faculty of Medicine, Osaka, Japan (Prof K Nakagawa MD); Tokyo Medical University Hospital, Tokyo, Japan (S Nagase MD); Kyushu University Hospital, Fukuoka, Japan (I Okamoto MD); National Cancer Center, Chiba, Japan (T Yamanaka PhD); Chugai Pharmaceutical Co Ltd, Tokyo, Japan (K Tajima MSc, R Harada BS); Izumi Municipal Hospital, Osaka, Japan (M Fukuoka MD); and Wakayama Medical University, Wakayama, Japan (Prof Nobuyuki Yamamoto MD)

Correspondence to: Prof Nobuyuki Yamamoto, Wakayama Medical University, 811-1, Kimitidera, Wakayama-shi, Wakayama 641-8509, Japan nbyamamo@wakayama-med.ac.jp

mutation-positive participants in the phase 3 BeTa study of second-line treatment of NSCLC (12 patients treated with erlotinib and bevacizumab and 18 with erlotinib alone), median progression-free survival with erlotinib plus bevacizumab in patients with *EGFR* mutation-positive disease was substantially higher than with erlotinib alone (17.1 months vs 9.7 months).^{16,17} However, this analysis was post-hoc and *EGFR* mutation status was not a prespecified stratification factor in this trial. Because of this limitation, we undertook this phase 2 trial to examine the combination of erlotinib and bevacizumab in patients with *EGFR* mutation-positive NSCLC.

Methods

Study design and patients

JO25567 was a randomised, open-label, multicentre, phase 2 study in patients with stage IIIB/IV (according to the 7th edition of the General Rule for Clinical and Pathological Record of Lung Cancer¹⁸) or recurrent NSCLC with activating *EGFR* mutations. Patients were enrolled from 30 centres across Japan.

Eligible patients had histologically or cytologically (excluding sputum cytology) confirmed stage IIIB/IV or postoperative recurrent non-squamous NSCLC with activating *EGFR* mutation (either exon 19 deletion or Leu858Arg mutation). Tumour samples were screened for *EGFR* mutation by PCR-based hypersensitive *EGFR* mutation testing in local laboratories, according to standard testing practices. Other criteria included age 20 years or older when giving informed consent; Eastern Cooperative Oncology Group performance status 0 or 1;

adequate haematological, hepatic, and renal function; and life expectancy 3 months or more at the time of registration. No previous chemotherapy for advanced disease was allowed, but postoperative adjuvant or neoadjuvant therapy of 6 months or more previously was allowed. Previous radiotherapy was also allowed, but only for non-lung lesions. Patients had to have one or more measurable lesion based on Response Evaluation Criteria in Solid Tumors (RECIST 1.1).

Major exclusion criteria included confirmation of Thr790Met mutation, presence of brain metastases, history or presence of haemoptysis or bloody sputum, any coagulation disorder, tumour invading or abutting major blood vessels, coexistence or history of interstitial lung disease, and previous receipt of *EGFR* inhibitors or VEGF receptor inhibitors.

This study was done in accordance with the Declaration of Helsinki and Good Clinical Practice guidelines. The study protocol was reviewed and approved by the institutional review boards of the participating institutions (appendix p 10), and written informed consent was obtained from all patients.

Randomisation and masking

Patients were randomly assigned (1:1) to receive either erlotinib plus bevacizumab or erlotinib alone with a dynamic allocation method. Central randomisation was done by a clinical research organisation (EPS Corporation, Tokyo, Japan). Patients were stratified according to sex (men vs women), disease stage (stage IIIB vs stage IV vs postoperative relapse), smoking history (never smokers or former light smokers vs others), and type of *EGFR* mutation (exon 19 deletion vs Leu858Arg mutation). All patients and investigators were unmasked to treatment allocation.

Procedures

Patients assigned to the erlotinib plus bevacizumab group received bevacizumab 15 mg/kg by intravenous infusion on day 1 of a 21-day cycle and erlotinib orally once daily at 150 mg/day, starting from day 1 of cycle 1. Patients in the erlotinib alone group received erlotinib orally once a day at 150 mg/day. Patients remained on treatment until disease progression or unacceptable toxicity. Changes to dose of erlotinib or bevacizumab because of adverse events were allowed, as per the protocol. The dose of bevacizumab was not to be reduced except when dose adjustment was needed because of change in bodyweight. Dose reduction of erlotinib was allowed for up to two doses (100 mg/day and 50 mg/day) in a stepwise decrease. After two steps of dose reduction, erlotinib was discontinued. Patients who required suspension of erlotinib for more than 3 weeks consecutively, or of bevacizumab for more than 6 weeks from the date of previous administration, were discontinued from study treatment. In the erlotinib plus bevacizumab group, if either drug was discontinued, the other could be

See Online for appendix

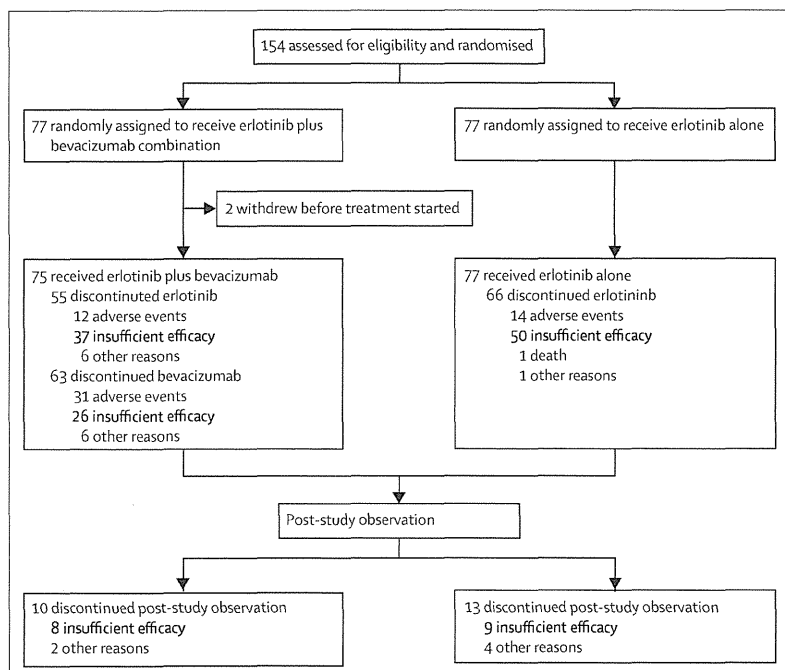


Figure 1: Trial profile

continued. Tumour lesions were assessed radiologically at baseline, week 4, week 7, every 6 weeks from week 7 to 18 months, and every 12 weeks thereafter until disease progression according to RECIST 1.1.

Patient-reported outcomes were assessed with the Functional Assessment of Cancer Therapy for patients with Lung cancer (FACT-L) scale until disease progression. An independent review committee of clinicians and radiologists masked to treatment assignment reviewed all tumour images and determined tumour response and progression status. Laboratory studies including blood and urine tests were done at days 1, 8, and 15 in cycles 1 and 2, and day 1 in cycle 3 and thereafter. Adverse events were monitored throughout the study period and were graded according to the National Cancer Institute Common Terminology Criteria for Adverse Events (CTC-AE) version 4.03.

Outcomes

The primary endpoint was progression-free survival, as determined by an independent review committee. Secondary endpoints were overall survival, tumour response (the proportion of patients with an objective response and disease control, and duration of response)

	Erlotinib plus bevacizumab group (n=75)	Erlotinib alone group (n=77)
Age (years)		
Median	67.0 (59-73)	67.0 (60-73)
<75	63 (84%)	62 (81%)
≥75	12 (16%)	15 (19%)
Sex		
Male	30 (40%)	26 (34%)
Female	45 (60%)	51 (66%)
Smoking status		
Never smoker	42 (56%)	45 (58%)
Former light smoker	9 (12%)	6 (8%)
Other	24 (32%)	26 (34%)
ECOG performance status		
0	43 (57%)	41 (53%)
1	32 (43%)	36 (47%)
Histopathological classification		
Adenocarcinoma	74 (99%)	76 (99%)
Large-cell carcinoma	0	1 (1%)
Adenosquamous carcinoma	1 (1%)	0
Clinical stage at screening		
IIIB	1 (1%)	0
IV	60 (80%)	62 (81%)
Postoperative recurrence	14 (19%)	15 (19%)
EGFR mutation type		
Exon 19 deletion	40 (53%)	40 (52%)
Exon 21 Leu858Arg mutation	35 (47%)	37 (48%)

Data are n (%) or median (IQR). ECOG=Eastern Cooperative Oncology Group.

Table 1: Baseline demographics and clinical characteristics

according to RECIST 1.1, quality of life, symptom improvement measured by the FACT-L scale, and safety profile.

Statistical analysis

A median progression-free survival of 13 months was estimated for the erlotinib alone group, and 89 events were deemed necessary to detect a hazard ratio (HR) of 0.7 in favour of erlotinib plus bevacizumab, with a one-sided significance level of 0.2 and a power of 0.8. The target sample size was set at 150 patients (75 patients in both groups), allowing for dropouts. Median progression-free survival was estimated by the Kaplan-Meier method and compared between groups with an unstratified log-rank test. Greenwood's formula was used to calculate 95% CIs. HRs were calculated by unstratified Cox proportional hazard methodology.

In the safety analysis, adverse events were converted to Medical Dictionary for Regulatory Activities (version 14.0) preferred terms, and tabulated by grade. Changes in laboratory test data with time were summarised in tables and graphs.

All patients who received at least one dose of the study treatment were included in the safety analysis population. The modified intention-to-treat population for the efficacy analysis included all patients who received at least one dose of study treatment and had tumour assessment at least once after randomisation. Statistical analyses were done with SAS version 9.2.

The study is registered with the Japan Pharmaceutical Information Center, number JapicCTI-111390.

Role of the funding source

The study was designed and funded by Chugai Pharmaceutical Co Ltd and monitored by a clinical research organisation (Niphix Corp, Tokyo, Japan) who

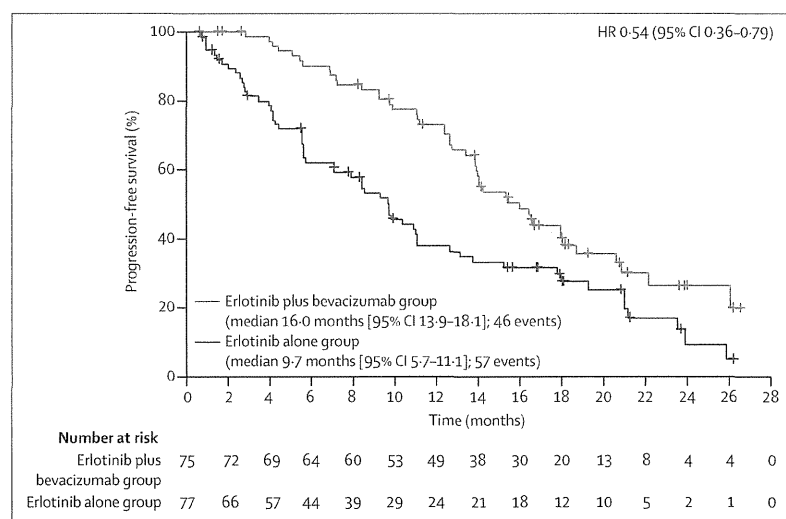


Figure 2: Progression-free survival, as determined by independent review committee, in the modified intention-to-treat population
HR=hazard ratio.

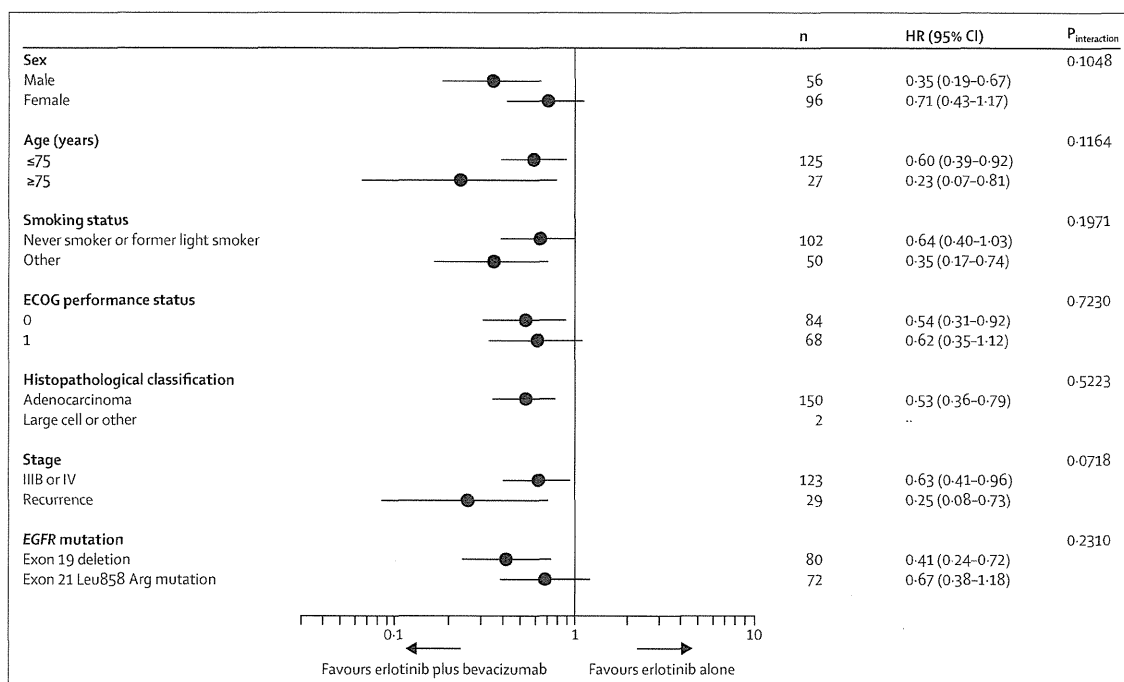


Figure 3: Forest plot of hazard ratios for progression-free survival by baseline characteristics. HR=hazard ratio.

	Erlotinib plus bevacizumab group (n=75)	Erlotinib alone group (n=77)
Complete response	3 (4%)	1 (1%)
Partial response	49 (65%)	48 (62%)
Stable disease	22 (29%)	19 (25%)
Progressive disease	0	6 (8%)
Non-evaluable	1 (1%)	3 (4%)

RECIST=Response Evaluation Criteria in Solid Tumors.

Table 2: Best RECIST response, as determined by independent review committee

obtained all data and did all initial data analyses; further analysis and interpretation was done by the funder, with input from the authors and investigators. The initial draft of the report was reviewed and commented on by all authors and by employees of Chugai Pharmaceutical Co Ltd. NobuY had full access to all data, and had final responsibility for the decision to submit the results for publication.

Results

Between Feb 21, 2011, and March 5, 2012, 154 patients were enrolled, of whom 77 were randomly assigned to receive erlotinib plus bevacizumab and 77 to erlotinib alone. Two patients withdrew before treatment started and were excluded (one had multiple thrombosis and the other had increased pleural effusion). Thus, data from 152 patients (75 patients in the erlotinib plus bevacizumab

group and 77 in the erlotinib alone group) were included in the analysis population (figure 1). The cutoff date for the primary analysis was June 30, 2013, when 103 progression events had occurred; median follow-up was 20.4 months (IQR 17.4-24.1).

The baseline characteristics of patients were well balanced between the groups (table 1). Median age was 67 years (IQR 60-73), and 27 (18%) patients were aged 75 years or older. EGFR mutation subtypes were balanced between the two groups.

Progression-free survival was significantly prolonged with erlotinib plus bevacizumab compared with erlotinib alone (log-rank test p=0.0015; figure 2). When subgroup analyses were done by baseline clinical characteristics, most patient subgroups seemed to have greater benefit from erlotinib plus bevacizumab compared with erlotinib alone. No significant difference was noted between any of the subgroups (p_{interaction}>0.05 for all subgroups; figure 3).

Analysis of progression-free survival by mutation subtype showed that in patients whose tumours had an exon 19 deletion (40 [53%] of 75 patients in the erlotinib plus bevacizumab group and 40 [52%] of 77 patients in the erlotinib alone group), median progression-free survival was significantly longer with erlotinib plus bevacizumab than with erlotinib alone (18.0 months [95% CI 14.1-20.6] vs 10.3 months [95% CI 8.0-13.1]; HR 0.41 [95% CI 0.24-0.72]; p=0.0011; appendix p 1). In patients whose tumours harboured the Leu858Arg mutation (35 [47%] patients in the erlotinib plus bevacizumab group; 37 [48%] patients in the erlotinib alone group), median

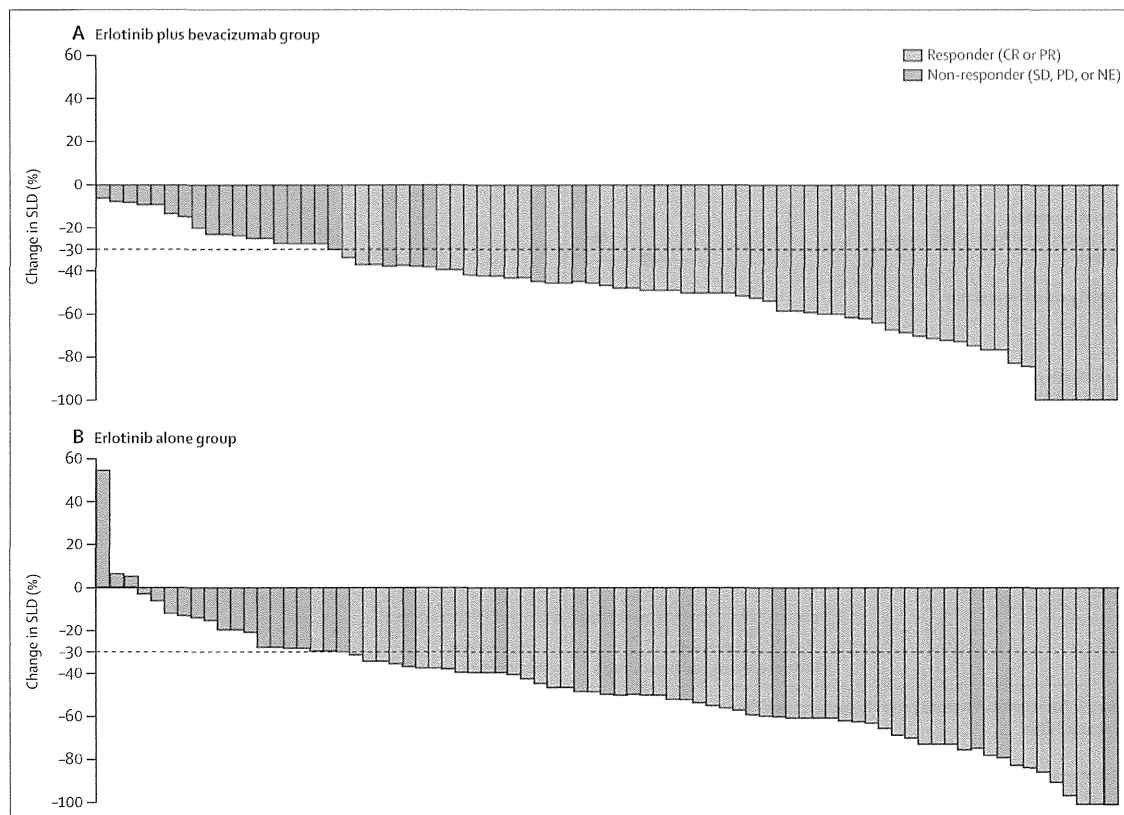


Figure 4: Waterfall plot of best percentage change from baseline in the sum of longest tumour diameters. Responders were confirmed by Response Evaluation Criteria in Solid Tumors. CR=complete response. PR=partial response. SD=stable disease. PD=progressive disease. NE=non-evaluable. SLD=sum of longest diameters.

progression-free survival was numerically longer with erlotinib plus bevacizumab than with erlotinib alone, but the difference was not significant (13.9 months [95% CI 11.2–20.9] vs 7.1 months [95% CI 4.3–15.2], respectively; HR 0.67 [95% CI 0.38–1.18]; $p=0.1653$; appendix p 2).

52 (69% [95% CI 58–80]) patients in the erlotinib plus bevacizumab group had an objective response, as did 49 (64% [52–74]) patients in the erlotinib alone group ($p=0.4951$), although median duration of response was not significantly longer with erlotinib plus bevacizumab than with erlotinib alone (13.3 months [95% CI 11.6–16.5] vs 9.3 months [6.9–13.8]; $p=0.1118$). A greater proportion of patients achieved disease control with erlotinib plus bevacizumab (74 [99%] vs 68 [88%]; $p=0.0177$). Best responses to treatment are shown in table 2.

Figure 4 shows change in tumour size from baseline in the two groups. All patients in the erlotinib plus bevacizumab achieved tumour reduction, but three patients in the erlotinib alone group did not. Of patients who had a 30% or greater reduction in tumour size during treatment, six (8%) patients in the erlotinib plus bevacizumab group and 12 (16%) patients in the erlotinib alone group did not meet the criteria for complete or partial response according to RECIST.

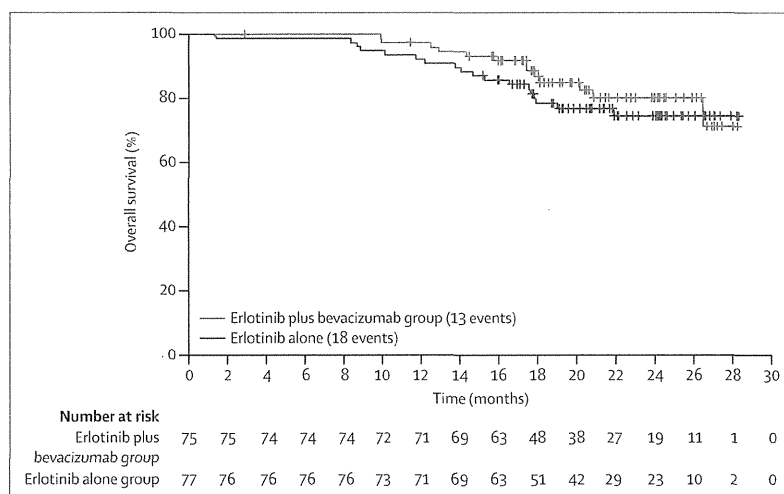


Figure 5: Overall survival, as determined by independent review committee, in the modified intention-to-treat population

Overall survival data are immature at present and so we cannot present any statistical analyses. At data cutoff, only 13 events (17%) had occurred in the erlotinib plus

	Erlotinib plus bevacizumab group (n=75)					Erlotinib alone group (n=77)				
	All	Grade 1-2	Grade 3	Grade 4	Grade 5	All	Grade 1-2	Grade 3	Grade 4	Grade 5
Rash	74 (99%)	55 (73%)	19 (25%)	0	0	76 (99%)	61 (79%)	15 (19%)	0	0
Diarrhoea	61 (81%)	60 (80%)	1 (1%)	0	0	60 (78%)	59 (77%)	1 (1%)	0	0
Paronychia	57 (76%)	55 (73%)	2 (3%)	0	0	50 (65%)	47 (61%)	3 (4%)	0	0
Dry skin	56 (75%)	54 (72%)	2 (3%)	0	0	45 (58%)	45 (58%)	0	0	0
Stomatitis	47 (63%)	46 (61%)	1 (1%)	0	0	46 (60%)	44 (57%)	2 (3%)	0	0
Haemorrhagic event	54 (72%)	52 (69%)	2 (3%)	0	0	22 (29%)	22 (29%)	0	0	0
Liver function disorder or abnormal hepatic function	33 (44%)	27 (36%)	5 (7%)	1 (1%)	0	39 (51%)	25 (32%)	7 (9%)	7 (9%)	0
Hypertension	57 (76%)	12 (16%)	45 (60%)	0	0	10 (13%)	2 (3%)	8 (10%)	0	0
Pruritus	34 (45%)	33 (44%)	1 (1%)	0	0	32 (42%)	32 (42%)	0	0	0
Weight decreased	33 (44%)	33 (44%)	0	0	0	19 (25%)	19 (25%)	0	0	0
Decreased appetite	26 (35%)	25 (33%)	1 (1%)	0	0	26 (34%)	25 (32%)	1 (1%)	0	0
Proteinuria	39 (52%)	33 (44%)	6 (8%)	0	0	3 (4%)	3 (4%)	0	0	0
Dysgeusia	20 (27%)	20 (27%)	0	0	0	17 (22%)	17 (22%)	0	0	0
Nasopharyngitis	20 (27%)	20 (27%)	0	0	0	15 (19%)	15 (19%)	0	0	0
Constipation	17 (23%)	17 (23%)	0	0	0	15 (19%)	14 (18%)	1 (1%)	0	0
Alopecia	13 (17%)	13 (17%)	0	0	0	14 (18%)	14 (18%)	0	0	0
Nausea	12 (16%)	12 (16%)	0	0	0	15 (19%)	15 (19%)	0	0	0
Vomiting	14 (19%)	14 (19%)	0	0	0	7 (9%)	7 (9%)	0	0	0
Malaise	10 (13%)	10 (13%)	0	0	0	10 (13%)	10 (13%)	0	0	0
Insomnia	8 (11%)	8 (11%)	0	0	0	8 (10%)	8 (10%)	0	0	0
Pyrexia	7 (9%)	7 (9%)	0	0	0	9 (12%)	9 (12%)	0	0	0
Upper respiratory tract infection	9 (12%)	9 (12%)	0	0	0	7 (9%)	7 (9%)	0	0	0
Conjunctivitis	8 (11%)	8 (11%)	0	0	0	7 (9%)	7 (9%)	0	0	0
Peripheral oedema	8 (11%)	8 (11%)	0	0	0	6 (8%)	6 (8%)	0	0	0
Fatigue	10 (13%)	9 (12%)	1 (1%)	0	0	3 (4%)	3 (4%)	0	0	0
Nail disorder	9 (12%)	9 (12%)	0	0	0	4 (5%)	4 (5%)	0	0	0
Dry eye	8 (11%)	8 (11%)	0	0	0	3 (4%)	3 (4%)	0	0	0
Dysphonia	8 (11%)	8 (11%)	0	0	0	1 (1%)	1 (1%)	0	0	0

Data are n (%).

Table 3: Adverse events reported by 10% or more patients for grades 1 and 2 and all adverse events for grades 3-5 (safety population)

bevacizumab group and 18 events (23%) in the erlotinib alone group (figure 5).

68 (91%) patients in the erlotinib plus bevacizumab group and 41 (53%) patients in the erlotinib group had grade 3 or 4 adverse events. The most common adverse events of any grade in the erlotinib plus bevacizumab group were rash, diarrhoea, hypertension, and paronychia, and in the erlotinib alone group were rash, diarrhoea, and paronychia (table 3). The most common grade 3 or worse adverse events in the erlotinib plus bevacizumab group were hypertension, rash, proteinuria, and liver function disorder or abnormal hepatic function, and in the erlotinib group were rash, liver function disorder or abnormal hepatic function, and hypertension (table 3). Substantially higher (>40%) incidences of hypertension, haemorrhagic events, and proteinuria were noted in the erlotinib plus bevacizumab group compared with the erlotinib alone group (table 3). Serious adverse events were reported by 18 (24%) patients in the erlotinib plus bevacizumab group and 19 (25%) patients in the erlotinib group.

12 (16%) patients in the erlotinib plus bevacizumab group and 14 (18%) patients in the erlotinib group discontinued erlotinib because of adverse events. 31 (41%) patients discontinued bevacizumab because of adverse events (figure 1). Ten patients discontinued both erlotinib and bevacizumab because of adverse events in the erlotinib plus bevacizumab group. Of these patients, seven discontinued erlotinib and bevacizumab simultaneously because of adverse events (liver function disorder or abnormal hepatic function in two patients, and infection, pancreatic cancer, rash, interstitial lung disease, and cerebral infarction in one patient each). In the remaining three patients, bevacizumab was initially discontinued, and patients continued on erlotinib monotherapy, although this was also subsequently discontinued. The dose of erlotinib was reduced to 100 mg for 34 (45%) of 75 patients in the erlotinib plus bevacizumab group and 33 (43%) of 77 patients in the erlotinib alone group; and to 50 mg for 17 (23%) of patients in the erlotinib plus bevacizumab group and eight (10%) patients in the erlotinib alone group.

The major adverse events leading to discontinuation of erlotinib in both groups were liver function disorder or abnormal hepatic function (two [3%] patients in the erlotinib plus bevacizumab group, eight [10%] in the erlotinib alone group), interstitial lung disease (two [3%], three [4%]), and rash (two [3%], none). Major adverse events leading to discontinuation of bevacizumab were proteinuria (11 [15%] patients), haemorrhagic events (nine [12%]), and hypertension (two [3%]). Most haemorrhagic events were low-grade epistaxis or haemorrhoidal bleeding. All of the 11 patients who discontinued bevacizumab because of proteinuria had grade 3 or lower events, and five of these patients recovered during the study period. All of the nine patients who discontinued because of haemorrhagic events had grade 3 or lower events; eight patients improved or recovered during the study period.

The median duration of erlotinib treatment was 431 days (range 21–837) in the erlotinib plus bevacizumab group and 254 days (18–829) in the erlotinib group, whereas median duration of bevacizumab was 325 days (1–815). The median duration of bevacizumab in patients who discontinued treatment because of proteinuria was 329 days (113–639) and because of haemorrhagic events was 128 days (23–357).

The relative dose intensity of erlotinib (calculated as [totally administered dose/total treatment duration]/150×100) was similar in both groups (95.3% [range 34.7–100.0] in the erlotinib plus bevacizumab group and 98.7% [33.3–100.0] in the erlotinib alone group), whereas that of bevacizumab (calculated as totally administered dose/planned dose×100) was 93.9% (72.4–99.7).

Haemoptysis was reported in six (8%) patients in the erlotinib plus bevacizumab group (five [7%] patients had grade 1 events and one [1%] had a grade 2 event); one patient (1%) had a grade 1 event in the erlotinib alone group. Interstitial lung disease was reported for five (3%) of all patients. One patient in the erlotinib alone group had grade 3 interstitial lung disease, but all other cases were grade 1 or 2, and all patients recovered. During the study period, one patient in the erlotinib group died by drowning, and a potential association with the study drug was confirmed.

No significant difference was noted between the two groups in terms of quality of life, including total FACT-L score, trial outcome index score, and all other subscores, since the standard deviations at each time point overlapped (appendix pp 3–9).

Discussion

In this study, the addition of bevacizumab to erlotinib significantly prolonged progression-free survival in patients with NSCLC with activating *EGFR* mutation-positive disease compared with erlotinib alone. To our knowledge, this is the first randomised study to show a clinically significant treatment effect of combining an *EGFR* tyrosine-kinase inhibitor with another biological

Panel: Research in context

Systematic review

We searched PubMed for articles published in English until Feb 1, 2014 (with no restrictions for the starting date), using the search terms “bevacizumab”, “erlotinib”, “NSCLC”, and “EGFR”. We identified two studies that had assessed the efficacy of erlotinib plus bevacizumab in the first-line setting.^{19,20} However, no previous study had assessed the efficacy of the combination of erlotinib and bevacizumab as first-line therapy for patients with activating *EGFR* mutation-positive NSCLC.

Interpretation

To our knowledge, this study is the first to show that the combination of erlotinib and bevacizumab can significantly prolong progression-free survival compared with erlotinib alone in patients with non-squamous *EGFR* mutation-positive NSCLC. Some degree of increased toxicity, particularly hypertension, proteinuria, and haemorrhagic events, was noted with the addition of bevacizumab. Our findings suggest that the combination of erlotinib and bevacizumab could be a new first-line regimen in *EGFR* mutation-positive NSCLC. Two clinical trials, BELIEF (NCT01562028) and ACCRU RC1126 (NCT01532089) are ongoing and the results are awaited to confirm the efficacy and safety shown in our study.

drug in patients with activating *EGFR* mutation-positive NSCLC (panel). We noted clear separation of the Kaplan-Meier survival curves from the start of treatment, despite the use of erlotinib in both groups.

Multivariate analysis according to baseline patient characteristics showed a consistent treatment benefit, with longer progression-free survival noted with erlotinib plus bevacizumab across most subgroups of patients. Previous studies have reported that erlotinib tends to be more effective in tumours with *EGFR* exon 19 deletions versus those with Leu858Arg mutations,^{7,8,21} which is consistent with our results.

No new safety signals were identified and the incidence of adverse events (any grade) and serious adverse events was similar between the two groups. There were more grade 3 or worse adverse events in the erlotinib plus bevacizumab group. Discontinuation of bevacizumab because of adverse events was more common than that reported in previous studies.^{13,14} One possible reason for this discrepancy could be the longer duration of treatment than in previous studies: the median treatment duration of bevacizumab was 325 days (16 cycles), which is substantially longer than that in previous studies. Furthermore, proteinuria was one of the major adverse events that led to discontinuation of bevacizumab, and the time to onset of bevacizumab discontinuation because of proteinuria tended to be in the later treatment phase (median 329 days [range 113–639]). Nevertheless, despite the high incidence of bevacizumab discontinuation because of adverse events, most of these events (mainly proteinuria and haemorrhagic events) were deemed non-serious and reversible.

The incidence of grade 3 or greater hypertension and proteinuria were higher than those in previous studies, again possibly related to the prolonged duration of treatment. Another potential factor that could explain the difference in the incidence of hypertension is in the

definition of grading used; we used CTC-AE version 4.03, whereas previous studies^{14,16} used CTC-AE version 3. Akhtar and colleagues²² showed that the change in CTC-AE version from 3 to 4 could lead to a significant shift in the severity of adverse events in clinical trials. Furthermore, despite the somewhat higher incidence of hypertension observed in this study, only two (3%) of 75 patients discontinued bevacizumab administration because of hypertension.

Although we noted no significant difference in the proportion of patients achieving an objective response between the erlotinib plus bevacizumab group and erlotinib alone groups, all patients in the erlotinib plus bevacizumab group had a reduction in tumour size. Of those patients who had a greater than 30% reduction in the sum of longest diameter of their target lesions from baseline, more patients in the erlotinib alone group failed to meet the criteria for complete or partial response. These findings suggest that the addition of bevacizumab to erlotinib might help to maintain the tumour-suppressing effect after reduction in tumour size, which might explain the difference in progression-free survival between the two groups.

One possible mechanism to explain this effect could be improved drug delivery. Bevacizumab changes tumour vessel physiology, resulting in increased intratumoral uptake of drugs.^{23,24} The results of a preclinical study suggested that patients on lower doses of EGFR tyrosine-kinase inhibitors tend to develop treatment resistance earlier than those who receive higher doses.^{25,26} Therefore, achieving a higher intratumoral concentration of erlotinib could delay the appearance of resistant cells. Another possible mechanism that could explain these findings is the effective blocking of angiogenesis signalling via the VEGF receptor and EGFR signalling pathways, which is thought to promote tumour growth.^{27,28} In addition to synergistic inhibition of tumour growth signalling, VEGF signal inhibition is still effective for tumours harbouring EGFR tyrosine-kinase inhibitor resistance mutations. In preclinical studies, blocking the VEGF receptor signalling pathway overcame resistance for EGFR signalling blockage by Thr790Met EGFR mutation *in vivo*.^{29,30}

Another treatment strategy that has been recently investigated is the combination of an EGFR tyrosine-kinase inhibitor with chemotherapy. Wu and colleagues³¹ reported that platinum doublet chemotherapy with intercalated erlotinib increased progression-free survival compared with platinum doublet chemotherapy alone. In a subset analysis of the EGFR mutation-positive population in this study, progression-free survival was 16.8 months. In our study, median progression-free survival with erlotinib and bevacizumab was 16.0 months. The first-line use of erlotinib and bevacizumab could allow chemotherapy to be reserved for subsequent lines of treatment, which might further improve survival outcomes in these patients.

Our study has several limitations. First, the analysis of EGFR mutations was not done at a central laboratory and

various methods were used, including the peptide nucleic acid, locked nucleic acid PCR clamp method, the PCR invader method, and the cyclecleave method. However, on the basis of previous evidence, these methods are generally judged to provide consistent results.³² Second, because some patients are still receiving the first-line treatment and overall survival data are still immature, assessment of subsequent treatment effects after progression is not possible. Data relating to post-study treatment will be reported in due course with updated overall survival results. Third, we did not use the EQ-5D questionnaire developed by the EuroQol group for quality-of-life assessment. Therefore, we could not formally estimate quality-adjusted life-years for a cost-effectiveness analysis. The health economics related to the combined use of erlotinib and bevacizumab remains unclear and should be discussed in future studies. Additionally, follow-up for overall survival is still ongoing and these results are needed before the clinical value of this combination can be determined.

In summary, our study provides, to the best of our knowledge, the first evidence that the addition of bevacizumab to erlotinib confers a significant improvement in progression-free survival when used as first-line treatment for patients with non-squamous NSCLC with activating EGFR mutation-positive disease. Some degree of increased toxicity, particularly hypertension, proteinuria, and haemorrhagic events, seems to be associated with the addition of bevacizumab. Our findings suggest that the combination of erlotinib and bevacizumab could be a new first-line regimen in EGFR mutation-positive NSCLC, and that further investigation of the regimen is warranted. Two clinical trials, BELIEF (NCT01562028) and ACCRU RC1126 (NCT01532089), are ongoing and the results are awaited to confirm the efficacy and safety shown in our study.

Contributors

NobuY was the principal investigator. TS, TK, MN, KG, NobuY, IO, TY, KT, RH, MF, and NobuY contributed to the study design and data analysis and data interpretation. TS, TK, MN, KG, SA, YH, NobuY, TH, MM, KN, SN, IO, and NobuY contributed to patient recruitment and data collection. NobuY, TS, KT, and RH prepared the initial draft of the report input from other authors. All authors approved the final version of the report.

Declaration of interests

TS received research grants and honoraria from Chugai Pharmaceutical. TK received research grants and honoraria from Chugai Pharmaceutical; honoraria from Eli Lilly, Ono Pharmaceutical, Novartis Pharma, Taiho Pharmaceutical, and AstraZeneca; and research grants from Nippon Boehringer Ingelheim, Kyowa Hakko Kirin, Pfizer, and Shionogi. MN received research grants and honoraria from Chugai Pharmaceutical, Pfizer, Novartis Pharma, Taiho Pharmaceutical, Nippon Boehringer Ingelheim, and AstraZeneca; research grants from MSD and Bristol-Myers Squibb. KG received research grants and honoraria from Chugai Pharmaceutical, Taiho Pharmaceutical and Nippon Boehringer Ingelheim; honoraria from AstraZeneca, Sanofi, Novartis Pharma, Pfizer, Yakult Honsha, Ono Pharmaceutical and Eli Lilly. SA received honoraria from Chugai Pharmaceutical, Eli Lilly, Taiho Pharmaceutical, Sawai Pharmaceutical, and Novartis Pharma. YH received research grants and honoraria from Chugai Pharmaceutical, Ono Pharmaceutical, and Taiho Pharmaceutical; honoraria from AstraZeneca, Eli Lilly, Novartis Pharma, and Takeda Pharmaceutical; research grants from Yakult Honsha, MSD, Kyowa Hakko Kirin, and Daiichi Sankyo. NobuY received research grants from Chugai Pharmaceutical, Pfizer, Takeda Bio, Astellas Pharma, Taiho

Pharmaceutical, and Bristol-Myers Squibb. TH received research grants from Chugai Pharmaceutical, AstraZeneca, Nippon Boehringer Ingelheim, Pfizer, Eli Lilly, Takeda Bio, Novartis Pharma, Ono Pharmaceutical, Daiichi Sankyo, Merck Serono, Kyowa Hakko Kirin, Dainippon Sumitomo Pharma, Bristol-Myers Squibb, and Eisai. MM received honoraria from Chugai Pharmaceutical and AstraZeneca; research grants and honoraria from Nippon Boehringer Ingelheim. KN received honoraria from Chugai Pharmaceutical, AstraZeneca, Nippon Boehringer Ingelheim, and Eli Lilly. SN declares no competing interests. IO received honoraria from Chugai Pharmaceutical, Eli Lilly, Pfizer, and Taiho Pharmaceutical. TY received honoraria from Chugai Pharmaceutical, Taiho Pharmaceutical, Takeda Pharmaceutical, and Bristol-Myers Squibb. KT and RH are employees of Chugai Pharmaceutical. MF received honoraria from Chugai Pharmaceutical. NobuY received honoraria from Chugai Pharmaceutical, Nippon Boehringer Ingelheim, and AstraZeneca.

Acknowledgments

We thank the patients, their families, and all of the investigators who participated in the study. Medical editorial assistance was provided by Rie Ishibashi and Damian Sterling from Nature Japan KK (Macmillan Medical Communications, Tokyo, Japan, funded by Chugai Pharmaceutical Co Ltd).

References

- WHO. 10 facts about cancer. <http://www.who.int/features/factfiles/cancer/en/> (accessed June 26, 2014).
- Lynch TJ, Bell DW, Sordella R, et al. Activating mutations in the epidermal growth factor receptor underlying responsiveness of non-small-cell lung cancer to gefitinib. *N Engl J Med* 2004; 350: 2129–39.
- National Comprehensive Cancer Network. NCCN Drugs & Biologics Compendium (NCCN Compendium). http://www.nccn.org/professionals/drug_compendium/content/contents.asp (accessed June 26, 2014).
- National Institute for Health and Care Excellence: Lung cancer (non small cell, EGFR-TK mutation positive)—erlotinib (1st line) (TA258). <http://guidance.nice.org.uk/TA258> (accessed June 26, 2014).
- Sequist LV, Yang JC, Yamamoto N, et al. Phase III study of afatinib or cisplatin plus pemetrexed in patients with metastatic lung adenocarcinoma with EGFR mutations. *J Clin Oncol* 2013; 31: 3327–34.
- Wu YL, Zhou C, Hu CP, et al. Afatinib versus cisplatin plus gemcitabine for first-line treatment of Asian patients with advanced non-small-cell lung cancer harbouring EGFR mutations (LUX-Lung 6): an open-label, randomised phase 3 trial. *Lancet Oncol* 2014; 15: 213–22.
- Zhou C, Wu YL, Chen G, et al. Erlotinib versus chemotherapy as first-line treatment for patients with advanced EGFR mutation-positive non-small-cell lung cancer (OPTIMAL, CTONG-0802): A multicentre, open-label, randomised, phase 3 study. *Lancet Oncol* 2011; 12: 735–42.
- Rosell R, Carcereny E, Gervais R, et al. Spanish Lung Cancer Group in collaboration with Groupe Français de Pneumo-Cancérologie and Associazione Italiana Oncologia Toracica: Erlotinib versus standard chemotherapy as first-line treatment for European patients with advanced EGFR mutation-positive non-small-cell lung cancer (EURTAC): A multicentre, open-label, randomised phase 3 trial. *Lancet Oncol* 2012; 13: 239–46.
- Macmondo M, Inoue A, Kobayashi K, et al. Gefitinib or chemotherapy for non-small-cell lung cancer with mutated EGFR. *N Engl J Med* 2010; 362: 2380–88.
- Mitsudomi T, Morita S, Yatabe Y, et al. Gefitinib versus cisplatin plus docetaxel in patients with non-small-cell lung cancer harbouring mutations of the epidermal growth factor receptor (WJTOG3405): an open label, randomised phase 3 trial. *Lancet Oncol* 2010; 11: 121–28.
- Fukuoka M, Wu YL, Thongprasert S, et al. Biomarker analyses and final overall survival results from a phase III, randomized, open-label, first-line study of gefitinib versus carboplatin/paclitaxel in clinically selected patients with advanced non-small-cell lung cancer in Asia (IPASS). *J Clin Oncol* 2011; 29: 2866–74.
- Sandler A, Gray R, Perry MC, et al. Paclitaxel-carboplatin alone or with bevacizumab for non-small-cell lung cancer. *N Engl J Med* 2006; 355: 2542–50.
- Reck M, von Pawel J, Zatlouk P, et al. Phase III trial of cisplatin plus gemcitabine with either placebo or bevacizumab as first-line therapy for nonsquamous non-small-cell lung cancer: AVAiL. *J Clin Oncol* 2009; 27: 1227–34.
- Niho S, Kunitoh H, Nokihara H, et al, for the JO19907 Study Group. Randomized phase II study of first-line carboplatin-paclitaxel with or without bevacizumab in Japanese patients with advanced non-squamous non-small-cell lung cancer. *Lung Cancer* 2012; 76: 362–67.
- Herbst RS, O'Neill VJ, Fehrenbacher L, et al. Phase II study of efficacy and safety of bevacizumab in combination with chemotherapy or erlotinib compared with chemotherapy alone for treatment of recurrent or refractory non small-cell lung cancer. *J Clin Oncol* 2007; 25: 4743–50.
- Herbst RS, Ansari R, Bustin F, et al. Efficacy of bevacizumab plus erlotinib versus erlotinib alone in advanced non-small-cell lung cancer after failure of standard first-line chemotherapy (BeTa): a double-blind, placebo-controlled, phase 3 trial. *Lancet* 2011; 377: 1846–54.
- Herbst R, Stern H, Amler L. Biomarker evaluation in the phase III, placebo-controlled, randomized BeTa Trial of bevacizumab and erlotinib for patients with advanced non-small cell lung cancer (NSCLC) after failure of standard 1st-line chemotherapy: correlation with treatment outcomes *J Thorac Oncol* 2009; 4: S323.
- The Japan Lung Cancer Society. General Rule for Clinical and Pathological Record of Lung Cancer, 7th edn. Tokyo: Kanehara Press, 2010.
- Zappa F, Droege C, Betticher D, et al. Bevacizumab and erlotinib (BE) first-line therapy in advanced non-squamous non-small-cell lung cancer (NSCLC) (stage IIIb/IV) followed by platinum-based chemotherapy (CT) at disease progression: a multicenter phase II trial (SAKK 19/05). *Lung Cancer* 2012; 78: 239–44.
- Dingemans AM, de Langen AJ, van den Boogaart V, et al. First-line erlotinib and bevacizumab in patients with locally advanced and/or metastatic non-small-cell lung cancer: a phase II study including molecular imaging. *Ann Oncol* 2011; 22: 559–66.
- Rosell R, Moran T, Queralt C, et al. Screening for epidermal growth factor receptor mutations in lung cancer. *N Engl J Med* 2009; 361: 958–67.
- Akhtar NH, Singh B, Ocean AJ, et al. Effect of CTCAE v4 grading of hypertension on reported toxicity in advanced cancer patient receiving vascular endothelial growth factor (VEGF)-targeting agents. *J Clin Oncol* 2013; 31: e15600.
- Wildiers H, Guetens G, DeBoeck G, et al. Effect of anti-vascular endothelial growth factor treatment on the intratumoral uptake of CPT-11. *Br J Cancer* 2003; 88: 1979–86.
- Dickson PV, Hamner JB, Sims TL, et al. Bevacizumab-induced transient remodeling of the vasculature in neuroblastoma xenografts results in improved delivery and efficacy of systemically administered chemotherapy. *Clin Cancer Res* 2007; 13: 3942–50.
- Furugaki K, Iwai T, Moriya Y, Harada N, Fujimoto-Ouchi K. Loss of an EGFR-amplified chromosome 7 as a novel mechanism of acquired resistance to EGFR-TKIs in EGFR-mutated NSCLC cells. *Lung Cancer* 2014; 83: 44–50.
- Hayakawa H, Ichihara E, Ohashi K, et al. Lower gefitinib dose led to earlier resistance acquisition before emergence of T790M mutation in epidermal growth factor receptor-mutated lung cancer model. *Cancer Sci* 2013; 104: 1440–46.
- Herbst RS, Johnson DH, Mininberg E, et al. Phase I/II trial evaluating the anti-vascular endothelial growth factor monoclonal antibody bevacizumab in combination with the HER-1/epidermal growth factor receptor tyrosine kinase inhibitor erlotinib for patients with recurrent non-small-cell lung cancer. *J Clin Oncol* 2005; 23: 2544–55.
- Larsen AK, Ouaret D, El Quadrani K, Petitprez A. Targeting EGFR and VEGF(R) pathway cross-talk in tumor survival and angiogenesis. *Pharmacol Ther* 2011; 131: 80–90.
- Naumov GN, Nilsson MB, Cascone T, et al. Combined vascular endothelial growth factor receptor and epidermal growth factor receptor (EGFR) blockade inhibits tumor growth in xenograft models of EGFR inhibitor resistance. *Clin Cancer Res* 2009; 15: 3484–94.
- Ichihara E, Ohashi K, Takigawa N, et al. Effects of vandetanib on lung adenocarcinoma cells harboring epidermal growth factor receptor T790M mutation in vivo. *Cancer Res* 2009; 69: 5091–98.
- Wu YL, Lee JS, Thongprasert S, et al. Intercalated combination of chemotherapy and erlotinib for patients with advanced stage non-small-cell lung cancer (FASTACT-2): a randomised, double-blind trial. *Lancet Oncol* 2013; 14: 777–86.
- Goto K, Satouchi M, Ishii G, et al. An evaluation study of EGFR mutation tests utilized for non-small-cell lung cancer in the diagnostic setting. *Ann Oncol* 2012; 23: 291–94.



Development of On-Chip Multi-Imaging Flow Cytometry for Identification of Imaging Biomarkers of Clustered Circulating Tumor Cells

Hyonchol Kim¹, Hideyuki Terazono^{1,2}, Yoshiyasu Nakamura³, Kazuko Sakai⁴, Akihiro Hattori¹, Masao Odaka¹, Mathias Girault¹, Tokuzo Arai⁴, Kazuto Nishio⁴, Yohei Miyagi³, Kenji Yasuda^{1,2*}

1 Kanagawa Academy of Science and Technology, Takatsu, Kawasaki, Japan, **2** Department of Biomedical Information, Division of Biosystems, Institute of Biomaterials and Bioengineering, Tokyo Medical and Dental University, Chiyoda, Tokyo, Japan, **3** Molecular Pathology and Genetics Division, Kanagawa Cancer Center Research Institute, Asahi-ku, Yokohama, Japan, **4** Department of Genome Biology, School of Medicine, Kinki University, Osaka-Sayama, Osaka, Japan

Abstract

An on-chip multi-imaging flow cytometry system has been developed to obtain morphometric parameters of cell clusters such as cell number, perimeter, total cross-sectional area, number of nuclei and size of clusters as “imaging biomarkers”, with simultaneous acquisition and analysis of both bright-field (BF) and fluorescent (FL) images at 200 frames per second (fps); by using this system, we examined the effectiveness of using imaging biomarkers for the identification of clustered circulating tumor cells (CTCs). Sample blood of rats in which a prostate cancer cell line (MAT-LyLu) had been pre-implanted was applied to a microchannel on a disposable microchip after staining the nuclei using fluorescent dye for their visualization, and the acquired images were measured and compared with those of healthy rats. In terms of the results, clustered cells having (1) cell area larger than 200 μm^2 and (2) nucleus area larger than 90 μm^2 were specifically observed in cancer cell-implanted blood, but were not observed in healthy rats. In addition, (3) clusters having more than 3 nuclei were specific for cancer-implanted blood and (4) a ratio between the actual perimeter and the perimeter calculated from the obtained area, which reflects a shape distorted from ideal roundness, of less than 0.90 was specific for all clusters having more than 3 nuclei and was also specific for cancer-implanted blood. The collected clusters larger than 300 μm^2 were examined by quantitative gene copy number assay, and were identified as being CTCs. These results indicate the usefulness of the imaging biomarkers for characterizing clusters, and all of the four examined imaging biomarkers—cluster area, nuclei area, nuclei number, and ratio of perimeter—can identify clustered CTCs in blood with the same level of preciseness using multi-imaging cytometry.

Citation: Kim H, Terazono H, Nakamura Y, Sakai K, Hattori A, et al. (2014) Development of On-Chip Multi-Imaging Flow Cytometry for Identification of Imaging Biomarkers of Clustered Circulating Tumor Cells. *PLoS ONE* 9(8): e104372. doi:10.1371/journal.pone.0104372

Editor: Thomas Dittmar, Witten/Herdecke University, Germany

Received: January 30, 2014; **Accepted:** July 10, 2014; **Published:** August 20, 2014

Copyright: © 2014 Kim et al. This is an open-access article distributed under the terms of the Creative Commons Attribution License, which permits unrestricted use, distribution, and reproduction in any medium, provided the original author and source are credited.

Funding: This work was supported by Kanagawa Prefector’s local basic science funding for the On-chip Cellomics Project at the Kanagawa Academy of Science and Technology. The funder had no role in study design, data collection and analysis, decision to publish, or preparation of the manuscript.

Competing Interests: The authors have declared that no competing interests exist.

* Email: yasuda.bmi@tmd.ac.jp

Introduction

Finding irregular cells in blood is fundamental to achieving non-invasive health checks, such as cancer and immune diagnostics. For example, circulating tumor cells (CTCs) are expected to form additional seeds for subsequent growth of tumors [1–3], and quantitative detection of CTCs in the blood [4–8] has the potential to achieve minimally invasive cancer diagnosis in comparison with conventional biopsies. One major approach to finding irregular cells is the targeting of specific molecules, molecular biomarkers, on the cell surface [1,3,6,9,10]; however, its application has sometimes had the difficulty of false-negative detection because of the variety of molecular expression properties of targeted cells.

To overcome these difficulties, we developed another system for the recognition of target cells [11–13]. In this system, cell samples were applied to a microchannel fabricated on a small microchip, cellular images were taken with a high-speed CCD camera, and target cells were identified depending on their morphological

characteristics, such as cellular area and perimeter. These morphological parameters, referred to as “imaging biomarkers” hereafter, are other indexes to identify specific target cells. For example, a large cellular size was indicated for some tumor cells [14–17], and a larger nucleus than in healthy cells is known as one common property of the morphometric phenotype of cancer cells [18–24]; therefore, finding target cells using imaging biomarkers, especially using both cell size and nucleus conformation, is useful for the identification of tumor cells. In this study, a real-time cell sorting system to achieve simultaneous processing of imaging biomarkers for both optical image (i.e., total cell configuration) and fluorescent image (i.e., nucleus configuration) was developed, and it was applied to identify irregular cells, especially clustered cells, in a blood sample. According to previous reports on CTC detection, the possibility of the CTCs forming clusters was suggested [7]; however, clear evidence had not been identified and there have been no quantitative studies on the identification of clustered cells in the blood. Here, a quantitative approach for cluster detection was suggested using imaging biomarkers as detection indexes.

Materials and Methods

Fabrication of microchip

The microchip was fabricated by the following procedure. A mask blank, which was a glass substrate coated with both chromium for light interception and positive photo-resist (AZP1350) for the fabrication of patterns (CBL4006Du-AZP, Clean Surface Technology Co., Kanagawa, Japan), was set to a laser lithography system (DDB-3TH, Neoark, Co., Tokyo, Japan) and a laser (405 nm wavelength) was irradiated onto the mask blank in the same pattern as the microchannel used in this study. After the irradiation, the mask blank was immersed in a developer of the resist (NMD-3, Tokyo Ohka Kogyo Co., Kanagawa, Japan) to remove the resist on which the laser was irradiated; then, a chromium layer was bared at this position. Next, the mask blank was immersed in chromium etching solution (MPM-E350, DNP Fine Chemicals, Co., Kanagawa, Japan), after which the bared chromium layer was removed and a transparent pattern of the microchannel was formed on the substrate. Finally, the whole resist on the mask blank was removed by light irradiation onto the whole of the substrate and immersion of the substrate in the developer; then, a photo mask of the microchannel was fabricated.

On the other hand, a light-curing resin (SU-8 3025, Nippon Kayaku Co., Tokyo, Japan) was spin-coated using a spin coater (1H-DX2, Mikasa, Co., Tokyo, Japan) of 25 μm thickness on a clean Si substrate. The resin-coated substrate was pre-baked at 95°C for 15 min, set in a mask aligner with the fabricated photo mask (MA-20, Mikasa), and the light (365 nm wavelength) was irradiated through the mask to harden the resin with the pattern of the microchannel. The substrate was heated at 65°C for 1 min and 95°C for 5 min sequentially to promote hardening of the resin, and excess resin was removed by immersing the substrate in SU-8 developer (Nippon Kayaku). A mold of the microchannel was then fabricated using the resin on the Si substrate.

To fabricate the chip, poly(dimethylsiloxane) (PDMS; SYLGARD 184 silicon elastomer, Dow Corning Co., Midland, MI, USA) was dropped onto the fabricated mold in solid state, and heated at 90°C for 1 h to harden the PDMS. The PDMS on which the pattern of the microchannel was transferred was peeled off from the mold and stuck with cleaned cover glass. Finally, plastic columns for the application of solvents including sample blood were pasted on the PDMS with epoxy resin; then, the microchip to be used in this study was fabricated.

Preparation of sample blood

This study was carried out in strict accordance with the Act on Welfare and Management of Animals of the Ministry of the Environment, Japan. The protocol was approved by the animal experiment committee of the Kanagawa Cancer Center (permit number 21-02). MAT-LyLu is a rat prostate cancer cell line established from the original Dunning R3327 tumor maintained by *in vivo* passage of a prostate cancer that spontaneously occurred in a Copenhagen rat [25]. This cell line was a generous gift from the original founders through Hisao Ekimoto, Ph.D., at the Oncology Section, Laboratory of Biology, Nippon Kayaku Co., Ltd., and was maintained in our laboratory.

To obtain blood containing cancer cells, the MAT-LyLu was adjusted to 5×10^6 cells in 200 μL of cell culture medium (RPMI 1640, Life Technologies Co., Grand Island, NY, USA), and implanted into the dorsal subcutaneous tissue of a Copenhagen rat (male, 6 weeks old). At 2 weeks after implantation, blood of the rat was collected from the subclavian vein using a collection tube containing heparin. The blood was hemolyzed using commercial reagent (BD Pharm Lyse, without fixative, BD Biosciences, San

Jose, CA, USA) for 10 min, washed along with $200 \times g$ centrifugation for 5 min and re-suspended two times in phosphate-buffered saline (PBS) containing 1% bovine serum albumin, suspended in PBS containing 100 ng/mL Hoechst 33258, and then incubated for 10 min to stain cellular nuclei. The sample was washed again along with centrifugation 3 times, suspended in 5% glucose solution, and applied to the sample inlet on the chip.

Flow cytometry

The prepared sample blood was applied to the sample inlet on a fabricated microchip with a sample volume of 50 μL in an assay. The same buffer with the sample cell suspension (i.e., 5% glucose) was also used as a sheath buffer, and was applied to the sheath buffer inlet. Air pressure was applied onto both sample and sheath buffer inlets simultaneously using a syringe pump to introduce these liquids into the microchannels. Before starting the experiments, flow velocity was calibrated by taking images of calibration beads using a CCD camera (Ditect Co., Tokyo, Japan) as the shift of bead position in the microchannel within a few frames of the images, and typically, 1 kPa pressure achieved flow velocity of about 3 mm/sec at the position after the meeting of sample and sheath flows. Multi-imaging observations of sample blood were then performed through the multi-view unit with 3 mm/sec flow velocity and 200 fps acquisition rate.

Comparative genomic hybridization analysis

Rat genome comparative genomic hybridization (CGH) microarray 244A (Agilent Technologies, Santa Clara, CA, USA) was used to perform array CGH on genomic DNA obtained from the MAT-LyLu cell line according to the manufacturer's instructions. A DNA sample obtained from liver tissue of a healthy Copenhagen rat was used as a reference. Genomic DNAs were extracted using a QIAamp DNA Mini kit (Qiagen, Hilden, Germany) according to the manufacturer's instructions. The DNA concentration was determined with PicoGreen dsDNA Quantitation Reagent (Life Technologies). Agilent Genomic Workbench (Agilent Technologies) was used to analyze chromosomal patterns using an ADM-2 algorithm setting a threshold of 5.0.

Copy number assay

The gene copy numbers for *csrp2* and *zdhhc17* were determined using TaqMan Copy Number Assays according to the manufacturer's instructions (Applied Biosystems, Foster City, CA, USA). The gene-specific primers and TaqMan probes were used in the experiments had the following sequences. Rat *csrp2* primers were: sense, 5'-GGACTAAATGGATTGATGCCACTCT-3'; antisense, 5'-GTCCCTGCTTCAAAGAACCCTGTCT-3'; probe, 5'-FAM-AAGAGCAAGAAGAAACCC-MGB-NFQ-3'. Rat *zdhhc17* primers were: sense, 5'-GCCCTACTGCATGCATGATACA-3'; antisense, 5'-GGGCTGTTTTGCA-CATGAAATTCAA-3'; probe, 5'-FAM-CTGGACAGCATCT-GCTAGTATAC-MGB-NFQ-3'. Rat *rpp40* primers were: sense, 5'-GTATGACACTGGCATGGAAGTCT-3'; antisense, 5'-CT-TGCAGGTCTCTGTGGAT-3'; probe, 5'-FAM-CCTGGC-AATCAAAGTTAGGCTTAG-MGB-NFQ-3'. Genomic DNAs obtained from collected samples using the cell sorting system were extracted using a QIAamp DNA Micro kit (Qiagen) according to the manufacturer's instructions. The DNA concentrations were determined with PicoGreen dsDNA Quantitation Reagent. Rat *rpp40* was used as an internal control. Genomic DNAs obtained from MAT-LyLu cell line and healthy rat liver were used as positive and negative controls, respectively.

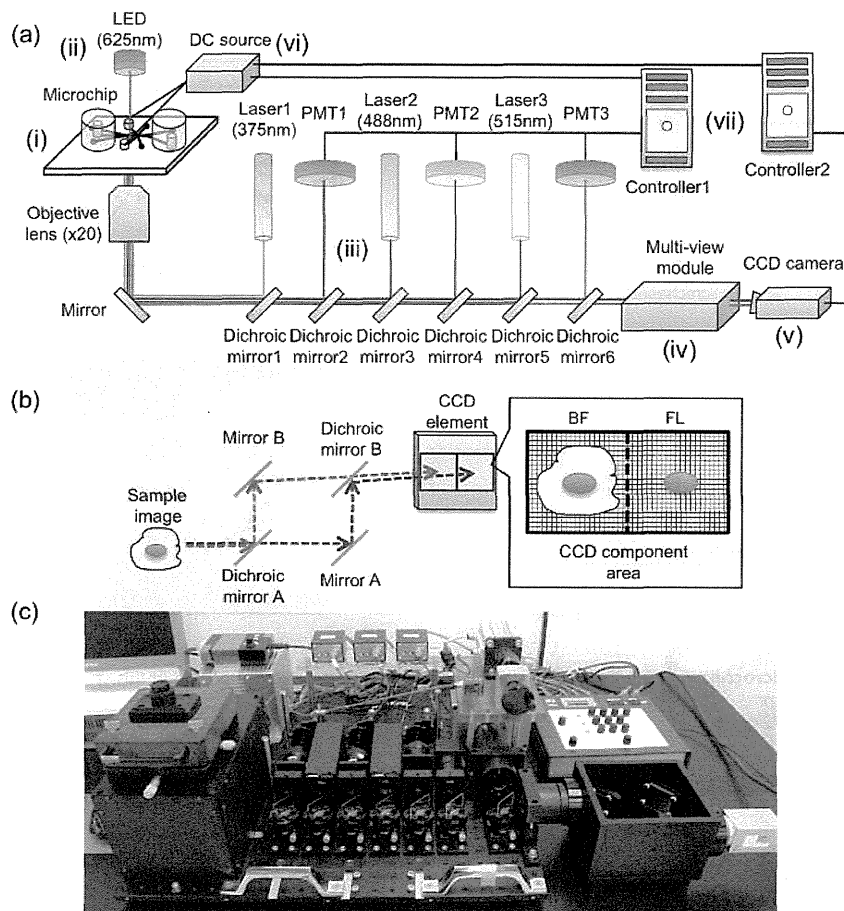


Figure 1. Instrumental set-up. (a) Summary of the on-chip multi-imaging flow cytometry system. The system was composed of seven major modules: (i) microchip, (ii) bright-field (BF) imaging, (iii) fluorescent (FL) detection, (iv) multi-view, (v) CCD camera, (vi) sorting, and (vii) controller, as numbered in the figure. (b) Summary of the multi-view module. (c) A photograph of the system. doi:10.1371/journal.pone.0104372.g001

Results

Development of on-chip multi-imaging flow cytometry system

The on-chip multi-imaging flow cytometry system (Fig. 1) was composed of seven major modules as an improvement of previous systems [11–13,26]: (i) microchip, (ii) bright-field (BF) light source, (iii) fluorescent (FL) excitation and detection, (iv) multi-view, (v) CCD camera, (vi) sorting, and (vii) controller, as numbered in Fig. 1 (a). In the BF light source module, an LED (625 nm wavelength) was used as a source for taking BF images and was irradiated from the top of the chip. This allowed simultaneous measurements of both BF and FL images, avoiding interference of the wavelengths during the measurements. An objective lens having 20 \times magnification and a 0.75 numerical aperture was set to the system, which allowed clear cell images to be taken within the depth range of the microchannel (25 μ m) [27]. The FL excitation and detection modules contained three excitation lasers (375, 488, and 515 nm) and photomultipliers (PMTs), respectively, to monitor three different FL signals, which allowed conventional FL detection with labeling of target biomarkers. The controller module consisted of two independent units: one calculated FL signals and the other processed imaging biomarkers in multi-view

images. Maximum frequencies of calculations were 10,000 frequencies per second (fps) for controller 1, which calculated FL intensities, and 200 fps for controller 2, which processed imaging biomarkers for the current system. According to the adjustment of suitable thresholds for these parameters, feedback signals could be sent to the sorting module. The sorting module was composed of a direct current (DC) source and electrodes connected with a microchip, and could apply DC voltages to cells flowing in a microchannel of the chip to purify target cells under feedback signals, if necessary. Figure 1 (b) shows the principle of the multi-view module [27,28] used in this study. Firstly, optical paths between BF (red) and FL (blue) lights were separated using dichroic mirror A, as indicated in the figure. Next, angles of mirrors A and B were adjusted; then, BF and FL images were projected onto each half of a CCD component in the camera. An overview of the total system is shown in Fig. 1 (c). The system has a desktop size of 60 cm \times 60 cm.

Figure 2 shows the microchip designed to be suitable for this study. The chip body was fabricated with poly(dimethylsiloxane) (PDMS) attached to a cover glass to apply optical transparency in the observation. Microchannels were placed between the PDMS and the bottom cover glass in the chip with a 2 mm ϕ buffer entrance penetrating the PDMS. The upper stream of the

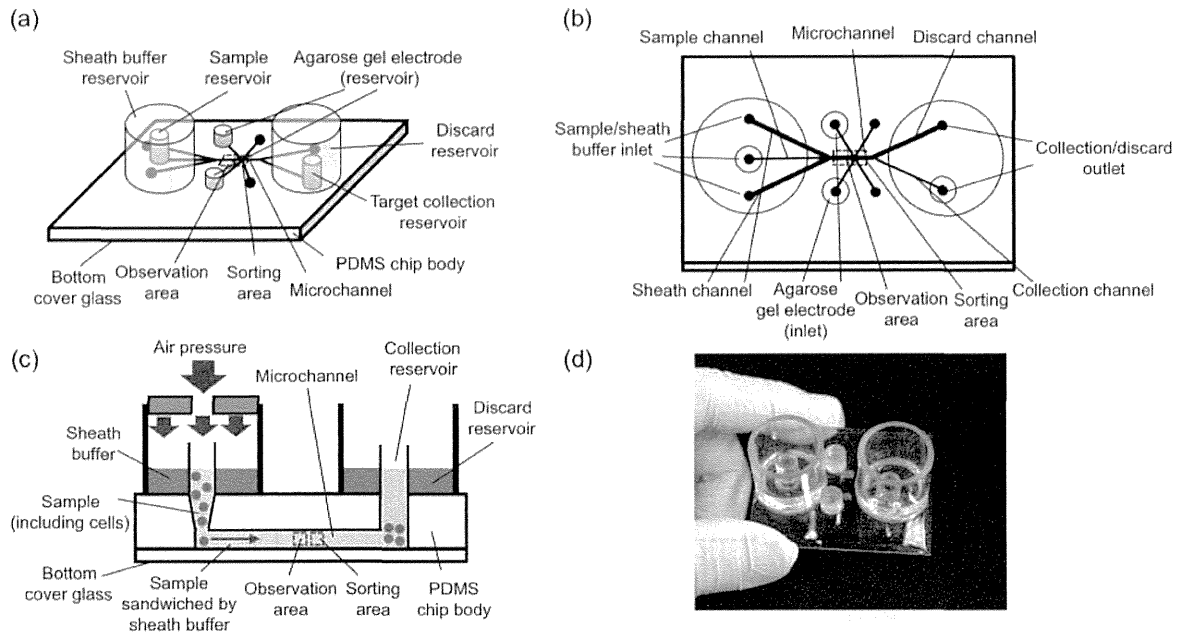


Figure 2. Overview of the microchip. (a) Diagonal, (b) top, and (c) side views of the microchip used in this study. (d) A photograph of the chip. Total chip size is 50 mm × 40 mm. doi:10.1371/journal.pone.0104372.g002

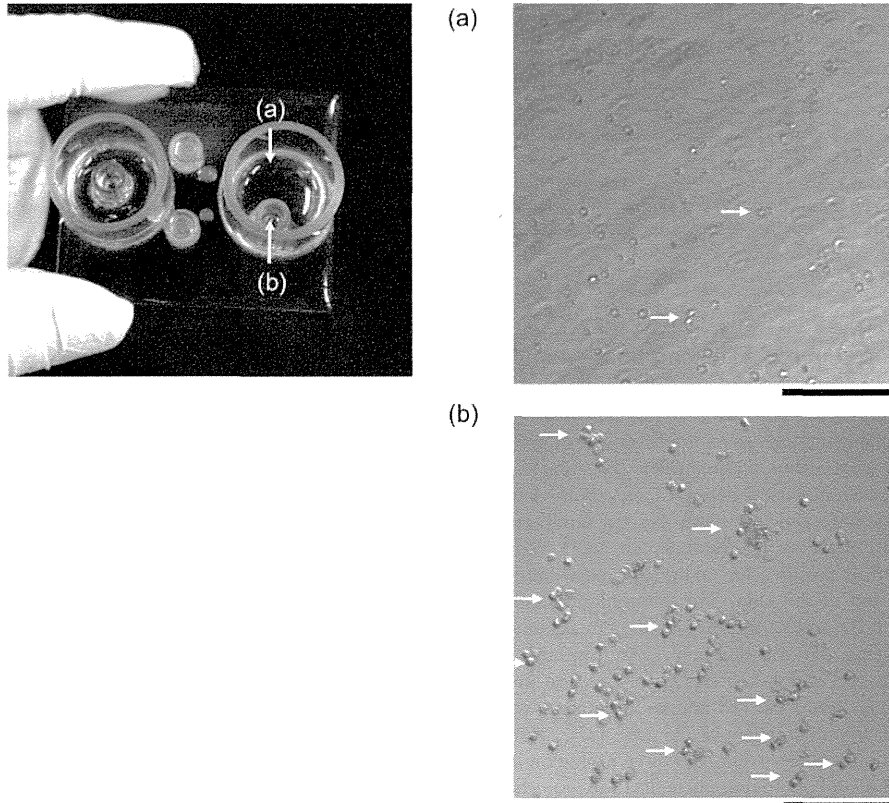


Figure 3. An example of cell sorting. Two photographs of the discarded reservoir (a) and the collection reservoir (b) indicated in the chip photograph are shown. Clustered cells are indicated by white arrows. Bars, 100 μ m. doi:10.1371/journal.pone.0104372.g003

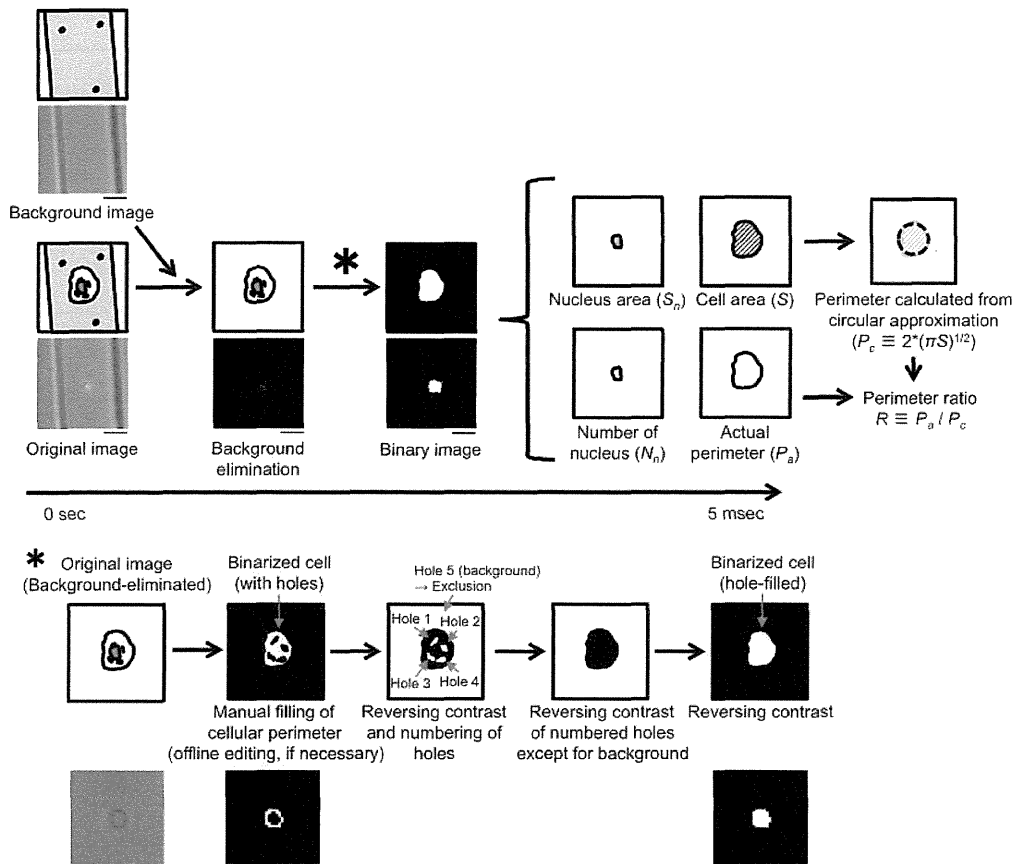


Figure 4. Summary of image processing. Firstly, photographs of both a cell and the background were taken. Next, the background image was subtracted from the cell image and holes were filled. Finally, imaging biomarkers, S , S_n , N_n , and R , were calculated. Bars, 10 μm . The hole-filling procedure is explained as indicated by an asterisk. Bar, 10 μm . doi:10.1371/journal.pone.0104372.g004

microchannel was branched into three channels: the center connected with the sample inlet and the others were a sheath buffer inlet. Both sample and sheath buffers were introduced into the channel with application of air pressure onto both sample and sheath buffer inlets, simultaneously (Fig. 2 (c)). After the meeting of sample and sheath flows, the width of the sample flow was focused in the central one-third, which allowed imaging of each single cell upon the arrangement of all the cells in a straight line.

Images of the linearly arranged cells were obtained through the multi-view module and processed by the system (see Fig. 1), and when a target cell was found, DC voltage (typically 40 V with 100 μsec length) was applied to the cell through the agarose gel electrode (Fig. 2 (a) and (b)) to change its course in the collection channel [11,13]. Figure 3 shows a typical example of the cell sorting with a blood sample of a cancer-implanted rat. As shown in this figure, target cells were set into cell clusters having a large BF area, and once the value of the BF area of the observed cell exceeded the pre-adjusted threshold value, 300 μm^2 in this model case, a sorting voltage was applied to the cell and, finally, target cells were collected into the target collection reservoir. Figures 3 (a) and (b) show pictures taken for discarding (a) and collection (b) reservoirs, respectively. As shown in Fig. 3 (b), large cell clusters (indicated by arrows in the figures) were collected into the collection reservoir. On the other hand, single cells or small cell clusters were collected into the discarding reservoir (Fig. 3 (a)),

indicating the success of target collection using one imaging biomarker, BF area, as a collection parameter. The sorting capacity, which has been determined as the ratio between the number of target cells automatically detected by the system and the actual number of cells in the collection reservoir, was 24%. The low capacity of target cell collection was caused by the higher threshold setting in both recognition and collection processes to prevent 'false positive' sample collection. When the commercially available microbeads were used as a model target in this system, sorting capacity increased to 91%.

As shown in Fig. 3, target cells can be recognized by comparison of the imaging biomarkers with the threshold values pre-adjusted in the system. Figure 4 shows the detail of image processing in the system to obtain imaging biomarkers. Firstly, a background image, which was taken before the assay of flow cytometry, was subtracted from the obtained image with reductions of 8-bit grayscale values in each pixel. Next, the subtracted image was transformed to a binary image using a suitable threshold and pixel errors in the cell, which appeared by almost the same contrast in the cell as in the background, were filled (Fig. 4, asterisk); then, an extracted cell image was obtained. Finally, imaging biomarkers were calculated from the extracted cell image. In the current system, cell area (S) and actual perimeter (P_a) were obtained from the BF image, and nucleus area (S_n) and number of nuclei (N_n) were obtained from the FL image.

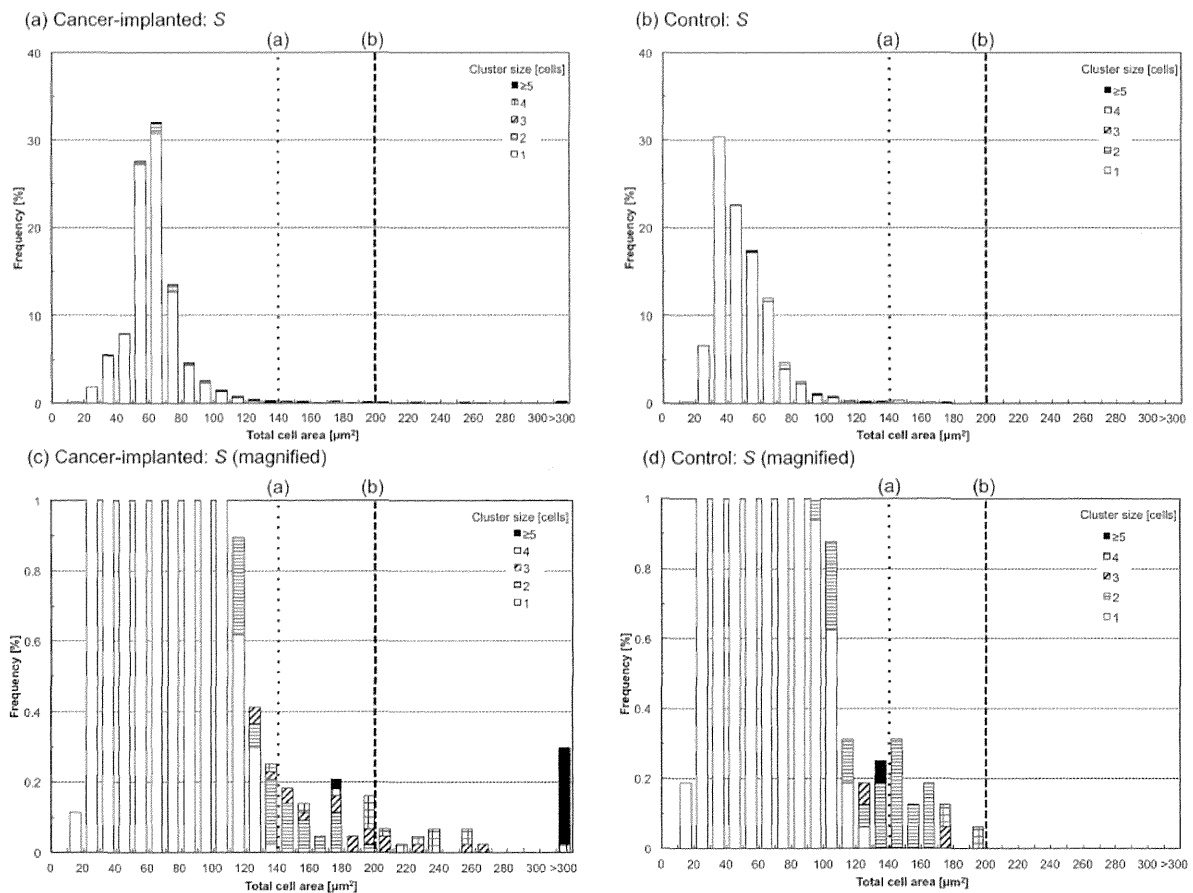


Figure 5. Histograms of total cell area, S , for cancer cell-implanted (a and c) and control blood (b and d). Two threshold values (a) and (b) for cluster identifications are indicated as dotted and dashed lines. doi:10.1371/journal.pone.0104372.g005

Additionally, the perimeter ratio, R , which was obtained as the ratio between P_a and the perimeter calculated from S (P_c) [29], was also obtained. These calculations were performed in real time at 200 fps using controller 2 in Fig. 1, and in this study, manual calculations of the imaging biomarkers, including a few modifications for apparently failed auto-calculations caused by the failure of continuous detection of the cell perimeter in the hole filling procedure, were also performed as post-processing to confirm the reliabilities of the obtained imaging biomarker values.

Detection of clustered cells in cancer-implanted rat blood using imaging biomarkers

After the success of the system development, its performance for the identification of specific target cells using imaging biomarkers was quantitatively evaluated. Blood of a rat in which a rat prostate cancer cell line (MAT-LyLu) had been implanted was chosen as a model sample, and clustered cells in the blood were set as a target for the detection using imaging biomarkers with the developed system. One approach anticipated to achieve successful detection of the clusters is the use of cell area; therefore, areas in BF images (i.e., total cell area, S) and FL images (i.e., total nucleus area, S_n) were measured using the system. Figures 5 and 6 are histograms of S (Fig. 5) and S_n (Fig. 6) for cells in the cancer-implanted blood ($N = 4375$), shown with healthy rat blood as its control ($N = 1599$).

Detailed numbers including S and S_n are also summarized in Table 1. From the results, clustered cells were observed at a count of 237 in cancer-implanted samples (5.4% of the total) and a count of 56 in the control (3.5% of the total). In addition, two clear threshold values were found in both S and S_n ; that is, (a) all cells having S larger than 140 μm^2 (count of 61, 1.4% of the total, for cancer-implanted samples and 13, 0.8% of the total, for the control) and S_n larger than 80 μm^2 (count of 34, 0.8% of the total, for cancer-implanted samples and 1, 0.1% of the total, for the control) were clustered cells, as indicated by the dotted lines in Figs. 5 and 6, and (b) the clustered cells having S larger than 200 μm^2 (count of 27, 0.6% of the total) and S_n larger than 90 μm^2 (count of 26, 0.6% of the total) were specifically observed in cancer cell-implanted blood. These results indicate that some cell clusters can be identified by using S and S_n (61 of 237, 26% of all clusters, for S and 34 of 237, 14% of all clusters, for S_n) as parameters for detection.

Obtained pictures were manually analyzed one by one with measured values of S and S_n . Figure 7 shows examples of single- and double-cell images having one, two, or three nuclei obtained from cancer-implanted and control blood, respectively. As shown in Fig. 7, the following 3 results were obtained: (i) single cells having multiple nuclei numbering more than two were specifically included in the cancer cell-implanted blood (count of 133, 3.2% of total single cells in cancer-implanted samples), (ii) two-cell clusters

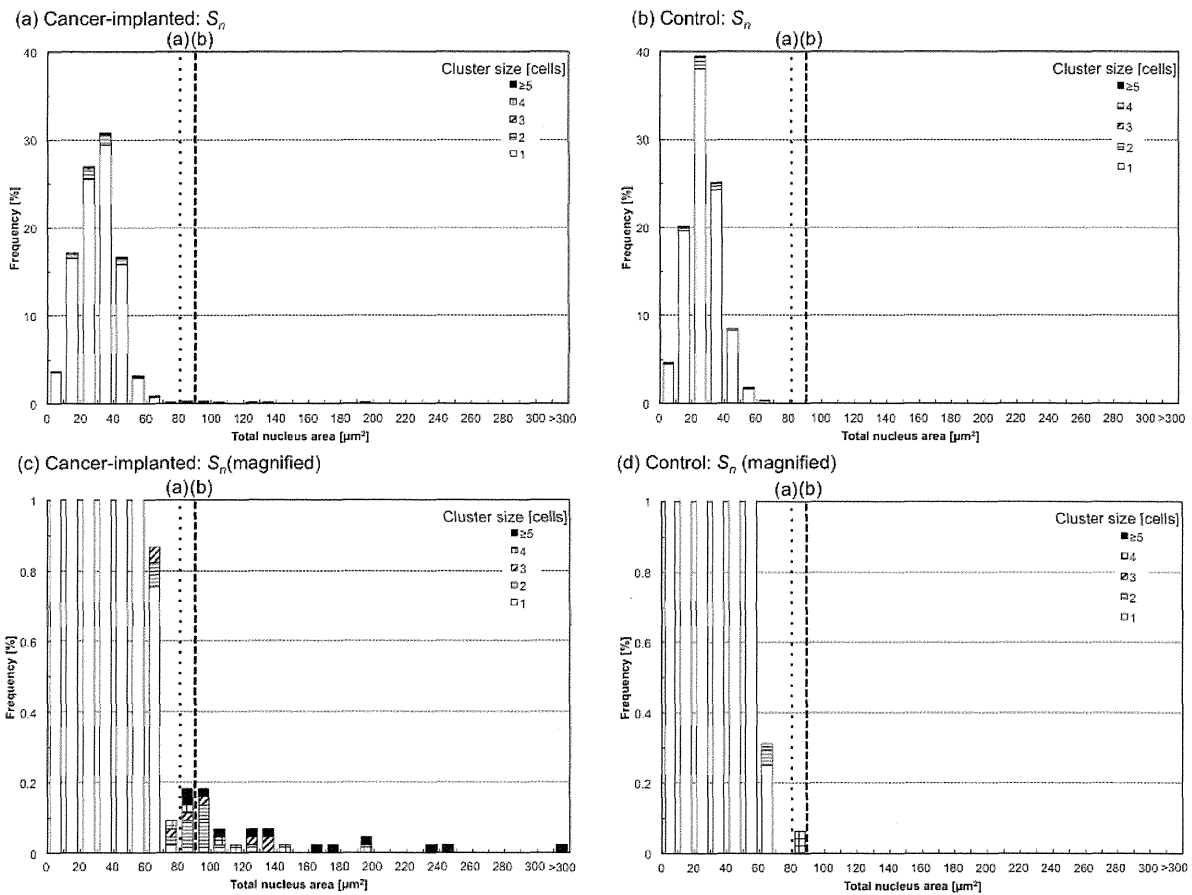


Figure 6. Histograms of total nucleus area, S_n , for cancer cell-implanted (a and c) and control blood (b and d). Two threshold values (a) and (b) for cluster identifications are indicated as dotted and dashed lines. doi:10.1371/journal.pone.0104372.g006

having only one nucleus seemed to be single cells to which a small particle (possibly debris of a hemolyzed red cell) was attached (count of 126, 72% of total two-cell clusters in cancer-implanted samples and count of 41, 84% of total two-cell clusters in control), and (iii) two-cell clusters having two nuclei were either true clusters or two independent cells flowing alongside each other (count of 48, including 2 clusters having 3 nuclei caused by the inclusion of a cell with multiple nuclei, 28% of total two-cell clusters in cancer-implanted samples and count of 8, 16% of total two-cell clusters in control). The first of these results shows the potential for the detection of implanted cancer cells having multiple nuclei, and the second can be thought of as single cells in general. The third in principle makes it difficult to distinguish two-cell clusters from two single cells using pictures; therefore, such two-cell “clusters” were also contained in control blood.

Figure 8 shows typical clustered cells composed of more than 3 cells. As shown in the figure and also in Table 1, a few clusters composed of more than 3 cells were also detected in control blood (count of 7 in total), with the maximum cell number of 6. However, they seemed to be single or two independent cells to which small particles were attached (i.e., the same as result (ii) in Fig. 7), which could also be confirmed by the number of nuclei, N_n , in the cluster, which had a maximum of 2. On the other hand, clusters contained in cancer-implanted blood were composed of more than 3 cells, with 15 cells at maximum, which was also

confirmed by N_n in the cluster being more than 3. It is unlikely for more than 3 cells to be flowing alongside each other; therefore, we concluded that clusters composed of more than 3 cells containing more than 3 nuclei were truly clustered cells in the blood. Such large clusters were contained in cancer cell-implanted blood at a count of 33 (7 counts, 21% of 3-cell clusters, 12 counts, 75% of 4-cell clusters, 14 counts, 100% of ≥ 5 -cell clusters, and 0.8% of the total). Measured values of N_n are summarized in Fig. 9 (a) (and also in Table 1). As shown in this figure, more than 99% of images in control blood had a single nucleus, and cell clusters having more than 3 nuclei were not contained in the blood. Figure 9 (b) also shows N_n summarized from the perspective of cluster size. As shown in the figure, large clusters in cancer-implanted blood had many nuclei, typically more than 3, indicating the possibility of the cluster formation of CTCs in the blood.

As shown in the above results, N_n is one useful imaging biomarker to identify cell clusters in blood; however, only using this marker for identification is insufficient because single cells having multiple nuclei were also contained in cancer cell-implanted blood, as shown in Fig. 7; therefore, we evaluated another imaging biomarker, perimeter ratio (R), for the identification of clustered cells. R is defined as the ratio between the actual perimeter obtained from the cell image and the perimeter calculated with a circle approximation of S . A low value of R indicates distorted conformation of the cell away from a circular

Table 1. Summary of total cell area, S , total nucleus area, S_n , number of nuclei, N_n , and perimeter ratio, R , for each cluster size.

Cancer-implanted (N=4375)			Total cell area, S [μm^2]					Total nucleus area, S_n [μm^2]				
Cluster [cells]	Frequency [counts]	Frequency [%]	Average	Median	S.D.	Max.	Min.	Average	Median	S.D.	Max	Min
1	4138	94.58	62	62	15	133	11	30	31	12	73	7
2	174	3.98	88	75	33	194	36	36	33	19	122	10
3	33	0.75	133	124	58	263	53	45	33	35	134	12
4	16	0.37	219	208	57	393	136	74	52	46	195	24
≥ 5	14	0.32	515	421	180	1163	179	149	131	85	342	37
≥ 2	237	5.4	129	81	130	1163	36	47	35	41	342	10
Cancer-implanted (continued)			Number of nuclei, N_n					Perimeter ratio, R				
Cluster [cells]	Frequency [counts]	Frequency [%]	Average	Median	S.D.	Max.	Min.	Average	Median	S.D.	Max	Min
1	4138	94.58	1.03	1.00	0.20	3	1	0.96	0.96	0.02	1.00	0.90
2	174	3.98	1.30	1.00	0.50	3	1	0.89	0.91	0.05	0.97	0.76
3	33	0.75	1.82	2.00	0.88	4	1	0.83	0.82	0.06	0.95	0.67
4	16	0.37	2.75	3.00	1.13	4	1	0.84	0.84	0.07	0.95	0.74
≥ 5	14	0.32	5.00	5.00	1.15	10	2	0.80	0.80	0.03	0.89	0.79
≥ 2	237	5.4	1.70	1.00	1.26	10	1	0.87	0.89	0.06	0.97	0.67
Control (N=1599)			Total cell area, S [μm^2]					Total nucleus area, S_n [μm^2]				
Cluster [cells]	Frequency [counts]	Frequency [%]	Average	Median	S.D.	Max.	Min.	Average	Median	S.D.	Max	Min
1	1543	96.50	48	44	16	121	11	27	26	10	69	7
2	49	3.06	99	83	36	169	40	28	28	12	61	7
3	3	0.19	119	127	62	177	54	23	24	10	32	13
4	2	0.13	187	187	14	197	177	51	51	43	81	20
≥ 5	2	0.13	116	116	24	133	99	32	44	18	57	32
≥ 2	56	3.5	104	88	39	197	40	29	28	14	81	7
Control (continued)			Number of nuclei, N_n					Perimeter ratio, R				
Cluster [cells]	Frequency [counts]	Frequency [%]	Average	Median	S.D.	Max.	Min.	Average	Median	S.D.	Max	Min
1	1543	96.50	1.00	1.00	0.00	1	1	0.96	0.96	0.02	1.00	0.90
2	49	3.06	1.16	1.00	0.37	2	1	0.82	0.84	0.05	0.91	0.70
3	3	0.19	1.67	2.00	0.58	2	1	0.83	0.83	0.06	0.89	0.77
4	2	0.13	1.50	1.50	0.71	2	1	0.81	0.81	0.08	0.86	0.75
≥ 5	2	0.13	1.00	1.00	0.00	1	1	0.81	0.81	0.01	0.82	0.80
≥ 2	56	3.5	1.20	1.00	0.40	2	1	0.82	0.83	0.05	0.91	0.70

doi:10.1371/journal.pone.0104372.t001

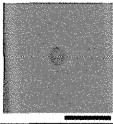
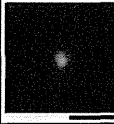
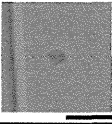
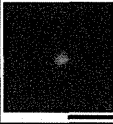
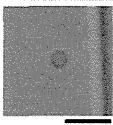
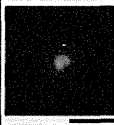
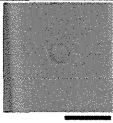
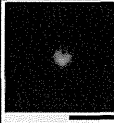
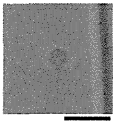
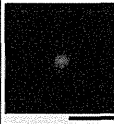
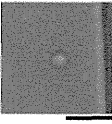
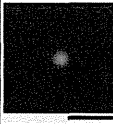
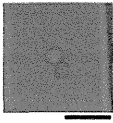
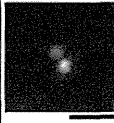
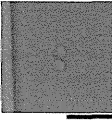
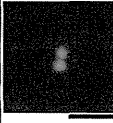
Cancer-implanted					Control				
Cluster size (N_n)	BF	FL	S [μm^2]	S_n [μm^2]	Cluster size (N_n)	BF	FL	S [μm^2]	S_n [μm^2]
1 (1) $n = 4005$			59	35	1 (1) $n = 1543$			55	21
1 (2) $n = 123$			57	41	1 (2)	N.A.			
1 (3) $n = 10$			72	47	1 (3)	N.A.			
2 (1) $n = 126$			67	26	2 (1) $n = 41$			69	40
2 (2) $n = 48$			117	74	2 (2) $n = 8$			73	61

Figure 7. Typical cell images for single and double cells in cancer cell-implanted and control blood. Each data count (n) indicates the image number having the same cluster size and N_n . Bars, 20 μm . doi:10.1371/journal.pone.0104372.g007

shape, which was expected for cell clusters. Figure 10 shows the relationship between the average value of R and cell cluster size for a cancer-implanted sample (detailed numbers are also shown in Table 1). As shown in the figure and table, all single cells had R higher than 0.90, with an average of 0.96, indicating that all cells having R smaller than 0.90 were clusters composed of more than 2 cells. On the other hand, R values for clusters composed of more than 2 cells were lower than 0.90 on average, and in detail, 131 clusters in cancer-implanted samples (55% of all clusters) and 55 clusters in control (98% of all clusters) had R lower than 0.90. Moreover, all large clusters composed of more than 3 cells having more than 3 nuclei, specifically observed only in cancer-implanted blood, had R lower than 0.90. These results indicate that more than half of the clusters, especially large clusters, could be identified by using R as an imaging biomarker.

According to the above results, large cluster formation of cancer cells in the blood was strongly expected. To confirm this, clusters larger than $300 \mu\text{m}^2$ were collected by performing cell sorting in the chip, and their cell types were identified by measuring genome errors in the cells. Firstly, target genes that were included in the MAT-LyLu chromosome with abnormal copy numbers were searched by comparative genomic hybridization (CGH) assay using the cell line, with liver tissue of the rat as a reference. Two particularly abundant genes, *csrp2* and *zdhhc17* located on chromosome 7q13, were found (Fig. 11 (a)) and set as target genes for the identification of cancer cells in the blood. Next, the TaqMan copy number assay was performed for cells collected in

both the collection reservoir and the discarded reservoir (see Fig. 3). From the results, increases of copy numbers for both *csrp2* and *zdhhc17* were specifically observed for clustered cells collected in the collection reservoir (Fig. 11 (b)). These results indicate that large clusters, which were specifically observed in cancer cell-implanted blood, were CTCs.

Discussion

In this study, four imaging biomarkers, cell area, nucleus area, number of nuclei, and perimeter ratio (S , S_n , N_n , and R), were evaluated for the identification of cell clusters in the blood. From the results, some threshold values were obtained for each imaging biomarker, namely, (1) S larger than $200 \mu\text{m}^2$ and (2) S_n larger than $90 \mu\text{m}^2$ were specific to cancer cell-implanted blood. In addition, (3) N_n higher than 3 was also specific to cancer cell-implanted blood. Finally, (4) all clustered cells composed of more than 3 cells having N_n higher than 3, which was specific to cancer cell-implanted blood, had R lower than 0.90. According to these results, the use of R is one useful approach for the identification of clustered cells having multiple nuclei numbering more than 3, which are specific to cancer cell-implanted blood. S and S_n are also useful parameters for the identification of extremely large clusters, which are quite likely to be CTCs. For small clusters composed of two cells, it is in principle difficult to distinguish whether the cluster is an actual cluster or two independent cells flowing alongside each other by using image-based analysis. One potential approach to distinguish these possibilities is the

Cancer-implanted					Control				
Cluster size (N_n)	BF	FL	S [μm^2]	S_n [μm^2]	Cluster size (N_n)	BF	FL	S [μm^2]	S_n [μm^2]
3 (3) $n = 6$			251	126	3 (1) $n = 1$			53	12
4 (4) $n = 4$			258	147	4 (1) $n = 1$			197	20
6 (6) $n = 1$			388	179	5 (1) $n = 1$			99	32
15 (max., 10) $n = 1$			1163	342	6 (max., 1) $n = 1$			133	50

Figure 8. Typical cell images for clustered cells composed of more than three cells in cancer cell-implanted and control blood. Each data count (n) indicates the image number having the same cluster size and N_n . Bars, 20 μm . doi:10.1371/journal.pone.0104372.g008

combination of the image-based analysis suggested in this study with a molecular analytical approach, such as quantitative gene copy number assays of the targeted cells. The system developed in this study has been combined with a cell sorting unit and can perform the combination measurement of multi-imaging analysis with molecular analysis, as shown in Fig. 11, which indicates the advantage of our developed system.

For the detection of CTCs, some methods were suggested. The principles were in general separated into two kinds; one was based on the chemical reaction and the other was physical detection. The former is in general based on the labeling of target molecules on the CTCs with antibodies, and it was sometimes combined with microfabrication technologies to improve detection sensitivities [6,7]. However, this approach sometimes yielded false-negative detection because of the variety of molecular expression levels in

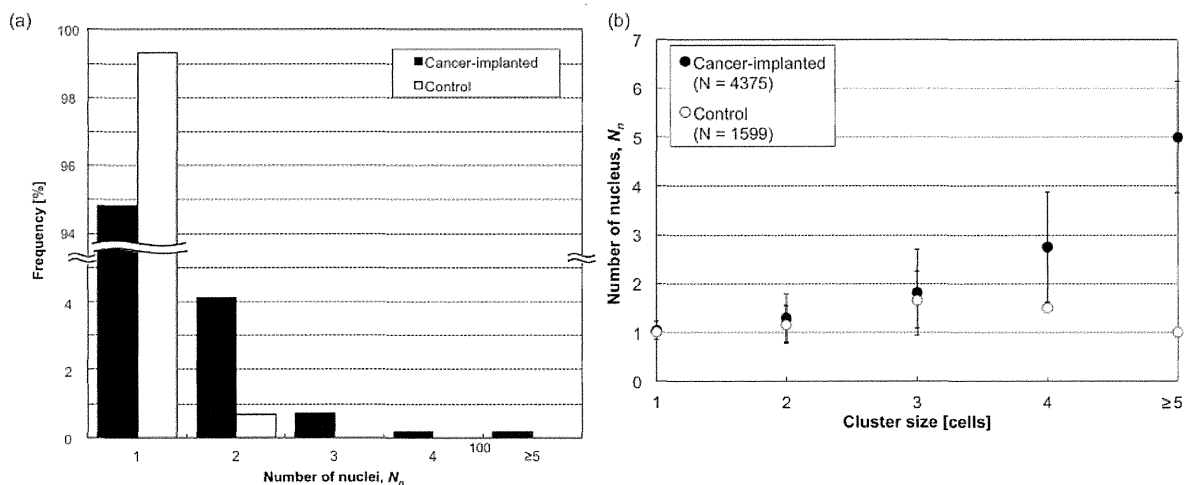


Figure 9. Summary of the number of nuclei, N_n . (a) A histogram of N_n obtained from cancer cell-implanted and control blood. (b) The relationship between N_n and cell cluster size. doi:10.1371/journal.pone.0104372.g009

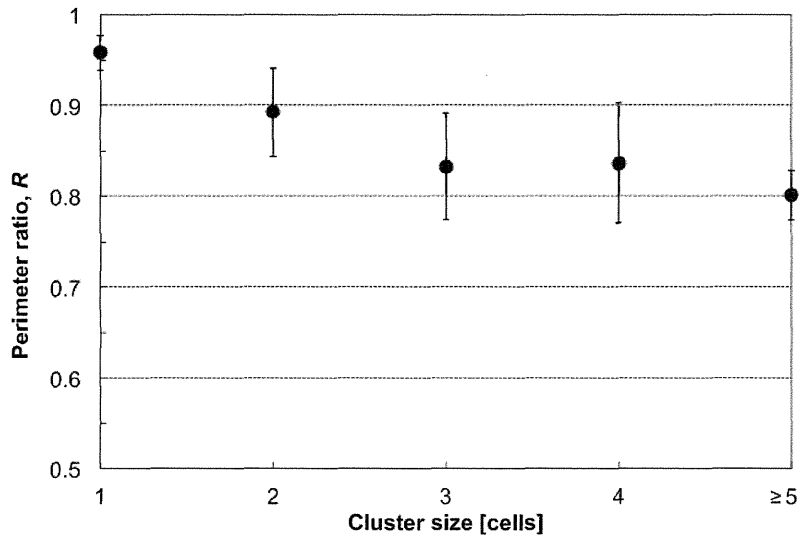


Figure 10. The relationship between perimeter ratio, R, and cell cluster size obtained from cancer cell-implanted blood.
doi:10.1371/journal.pone.0104372.g010

CTCs. For this latter case, various physical parameters of CTCs such as cell diameter [4,16,17] and dielectrophoretic properties [5] have been used with a combination of microfabrication technologies. According to the results in this study, cell size (*S*) is one useful parameter to find irregular cells in blood samples such as

clustered cells; however, the use of only one parameter is insufficient for the exhaustive detection of CTCs. Our developed system can use various parameters including both chemical and physical properties to find target cells, which would also be useful for the detection of various CTCs.

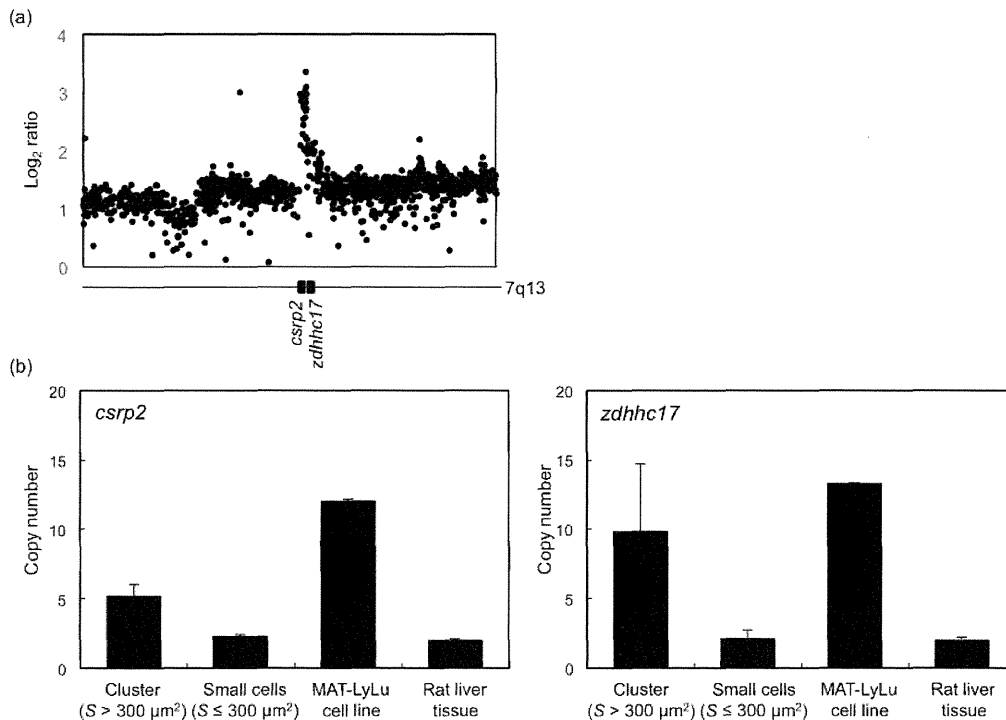


Figure 11. Results of quantitative gene copy number assays. (a) Results of CGH assays performed for the MAT-LyLu cell line. Liver tissue of the rat was used as a reference. Gene amplifications for *csrp2* and *zdhhc17* located on chromosome 7q13 were found. (b) Results of TaqMan copy number assays performed with clusters larger than 300 μm² collected in the collection reservoir, and cells smaller than 300 μm² collected in the discarded reservoir. Results of the assays for the MAT-LyLu cell line (positive control) and liver tissue (negative control) are also shown.
doi:10.1371/journal.pone.0104372.g011